UNIVERSITÉ DE NANTES
FACULTÉ DES
SCIENCES ET TECHNIQUES

icam
L'art et la manière de faire monde
Enseignement supérieur
Formation professionnelle
Services entreprises

MASTER THESIS

MODELING AND NUMERICAL SIMULATION OF TWO THERMO-MECHANICAL INDUSTRIAL PROCESSES: IMPACT WELDING AND FUSION WELDING

Student: Inès GHORBEL
Master 2 Computational Mechanics 2016-2017

ICAM adviser: Amaury DELDICQUE
UN adviser: Professor Marc FRANÇOIS

Acknowledgment

At the end of this modest work we would like to express our sincere thanks to:

M. Amaury DELDICQUE, *our advisor for this internship at the* ***C****atholic* ***I****nstitute of* ***A****rts and* ***C****rafts Icam school in Lille for his support and guidance throughout the project, and his expertise in numerical simulation.*
We would also like to thank all the people of the Mechanical department at Icam.

M. Marc FRANÇOIS, *our academic referent in Nantes University for its pedagogy and all the knowledge that he has been able to bring me throughout my training.*

At the end, I thank all our professors in Nantes University for their courses and their disponibility.

Contents

Figures List

Tables List

Chapter1:

Introduction

1. General Presentation

The catholic Institute of arts and craft (Icam), is an engineering school funded in 1898 in Lille by the society of Jesus. It delivers Engineering degree (Master level) and offers also vocational trainings in engineering: lectures and qualification internships in R&D projects (for both short and long periods), research activities, cooperative programs.

Icam possesses 120 years of experience, 30 M€ of budget, 300 collaborators, 4000 between students, learners and trainers and 11500 engineering alumni. 9 campus exist in the world (figure 1): 6 in France (Lille, Paris Sénart, Nantes, Bretagne, Vendée and Toulouse) and 3 abroad (Pointe-Noire and Douala in Africa and Chennai in India).

Figure 1. Different campus of Icam School [1]

Icam has 4 poles: High education, Professional training, Business services and support.

Icam School has four research teams:

- One with Group responsibilities: taking care of strategy, scientific and technological development, but especially, the pooling of resources and skills, the capitalization of experiences and the provision of appropriate means.
- Three with regional and local responsibilities: At the heart of their respective regions, they are responsible for the operational and administrative aspects of our research projects, all supporting our companies and laboratories.

6 main axes of research have been defined:

- Axe 1: Energy storage and management
- Axe 2: Industrial co-products and waste recycling
- Axe 3: Innovative materials and treatments
- Axe 4: Structures and couplings

- Axe 5: Industrial, environmental and societal changes
- Axe 6: Factory 4.0

Also, Icam has 3 types of partners which are:

- Academic partners:
  - ✓ CNRS
  - ✓ Ecole Centrale of Nantes
  - ✓ Nantes' university
  - ✓ INRIA
  - ✓ Catholic University of Lille
  - ✓ Etc
- Industry partners:
  - ✓ Renault
  - ✓ Airbus
  - ✓ SMTC
  - ✓ Volvo
  - ✓ CNES
  - ✓ Etc
- International partners :
  - ✓ University of Exeter, UK
  - ✓ University of Limerick, Ireland
  - ✓ GAIKER Centro Tecnológico, Spain
  - ✓ Universitat Politècnica de València, Spain
  - ✓ University of Deusto, Spain

2. Icam Lille Campus

Icam Lille campus (figure 2) was the first campus funded in 1898. It possesses many departments (Mechanics, Materials, IT, …).

Figure 2. Icam Lille Campus

The mechanic and material department are now part of the Join'EM project which is an EU project started in September 2016. It addresses the increasing requirements of the industry to join dissimilar materials (aluminum and copper) which can be achieved by electromagnetic pulse welding process.

The following work which belongs the Icam's axe is the microscopic modelling of the Electromagnetic pulse welding. The aim of my internship is to simulate two cases of the Join'EM project (V112 and V82) and to validate this last with the experience from Fraunhofer which is also part of this project. After the validation of the impact welding, we study the fusion.

Chapter 2:

Literature Review

1. Introduction

Welding is an ancient art which has existed since the bronze age. It produces a joint that is stronger than other technologies of bonding metals. It is used in many industries including construction, oil and automotive.
In order to better understand this process, a literature review has been made and presented in this chapter.

2. Welding

Welding is a material joining process which produces combinate materials by heating them to suitable temperatures with or without the application of pressure or by the application of pressure alone, and with or without the use of filler material. Welding is used for making permanent joints. It is used in the manufacture of automobile bodies, aircraft frames, railway wagons, machine frames, structural works, tanks, furniture, boilers, general repair work and ship building.
Welding like all processes, have advantages and limitations which are illustrated in table 1.

Table 1. Advantages and limitations of welding process

Advantages	Limitations
Welding is a permanent joint	Edge preparation is required before welding
Efficiency of weld joint is 100%	Welding is inherently dangerous
A lot of similar and dissimilar metal can be join by welding	Thermal stress is produce in the weld material
Cost of welding joint is very economical	Heat treatment process is required to remove these stresses

To ensure a good welding, the weld joint must be designed to withstand the forces under gone its service life. Some types of welding joints are designed to withstand extreme shear loads, while others are designed to withstand extreme torsional loads. Types of joints used for welding are butt, lap, corner, T, and edge (figure 3).

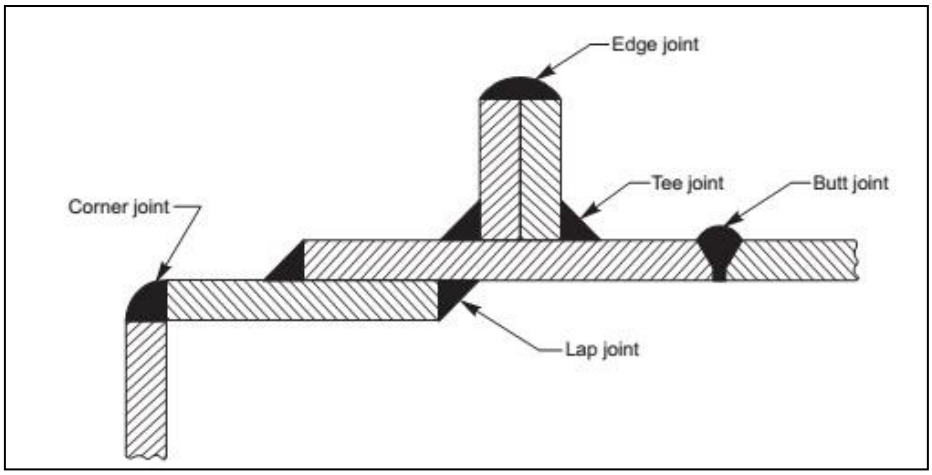

Figure 3. Divers types of joints [2]

The type of joint to be created and the type of material to be used, among other considerations, will determine the type of welding process that will be used to complete the project. All welding processes can be broken down into the two following categories as illustrated in figure 4.

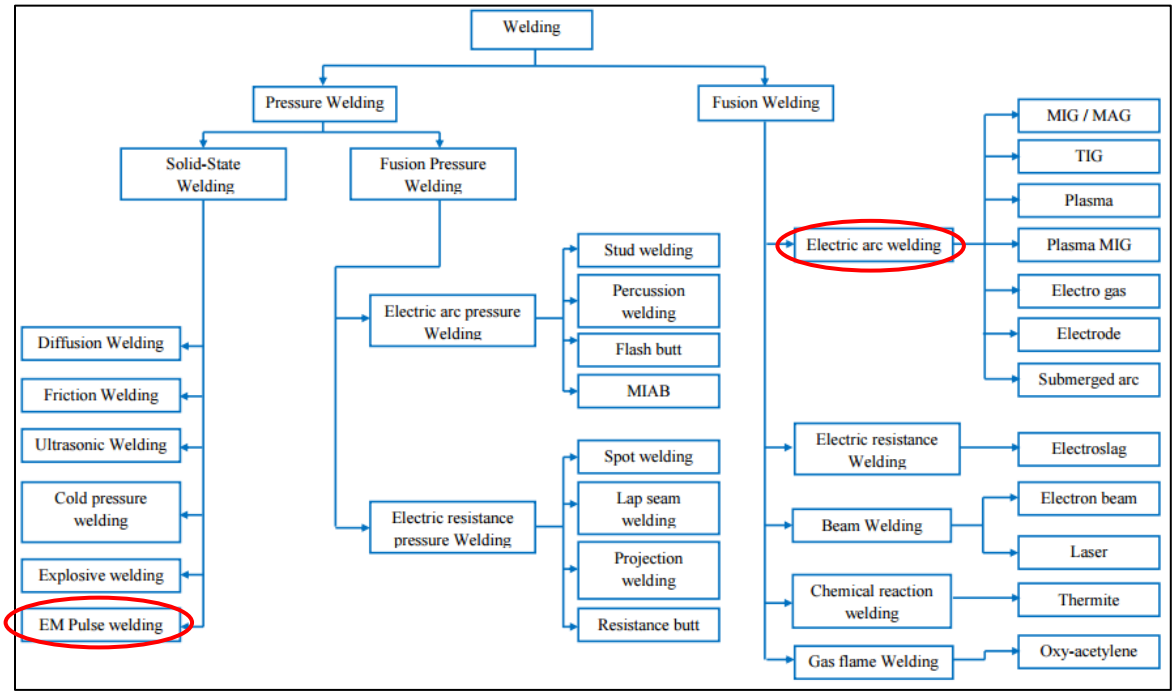

Figure 4. Classification of welding process based on the energy source

2.1. *Pressure Welding*

A pressure welding is a process in which the pressure is applied to produce the welding joint with a temperature below the melting Temperature. That's why it's also called solid state welding. Pressure welding techniques are used primarily on metals that are highly ductile or whose ductility increases with increasing temperature.

These different welding processes which fall in this category be introduce in the next section.

2.1.1. Explosive welding (EXW)

Explosive welding (figure 5) was the first industrial process application of impact welding. It has been widely used for its capability to join a wide variety of both similar and dissimilar metals.

This method is based on an explosive detonation in order to propel a flyer plate towards a base plate.

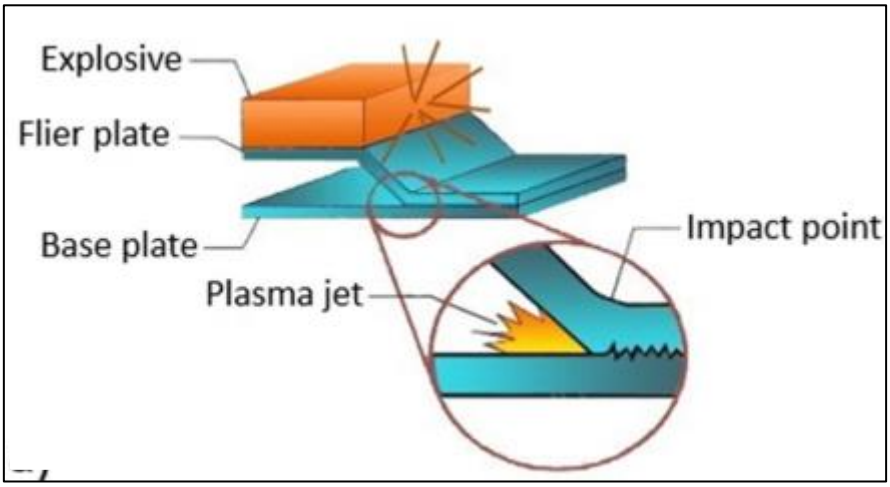

Figure 5. Explosive welding process [3]

Figure 6 shows the different parameters of this process where U_d is the detonation velocity, V_w is the welding velocity, V_p is the flyer plate velocity, V_f is flyer plate velocity observed at stagnation point, the V_j is the re-entrant jet velocity, the V_s is the slug velocity. The angles defined are α the angle of incidence, β the impact angle and δ the bending angle. The thicknesses given are t_p the flyer plate thickness, t_s the slug thickness, t_j the jet thickness.

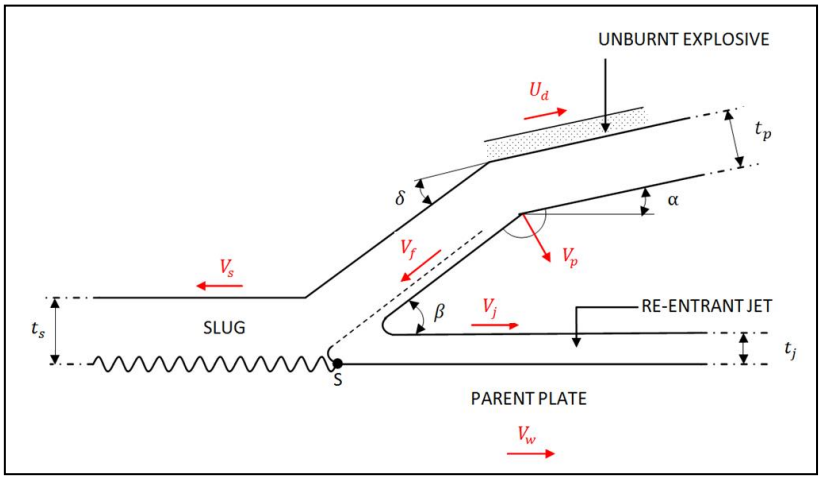

Figure 6. Explosive welding parameters [4]

The relationships between the various velocities and angles are as follows:

$$\frac{V_p}{\sin\beta} = \frac{V_w}{\cos\frac{1}{2}\delta} = \frac{V_f}{\cos\frac{1}{2}(\alpha+\beta)}$$

The duration and the acceleration of the process is defined with:

$$t = \frac{2g}{V_w}$$

$$a = \frac{{V_w}^2}{2g}$$

where g is the initial gap between the two plates.
The remaining velocities, for the slug and the jet as well as their masses can now be written:

$$V_j = V_f + V_w = \frac{V_p}{\sin\beta}(\cos\frac{1}{2}\delta + \cos\frac{1}{2}(\alpha+\beta))$$

$$V_s = V_f - V_w = \frac{V_p}{\sin\beta}(\cos\frac{1}{2}\delta - \cos\frac{1}{2}(\alpha+\beta))$$

The critical impact pressure is an important characteristic of the welding process and can be expressed in the following equation:

$$P_c = \frac{\rho_m {V_w}^2}{2}$$

Where Pc is the critical impact pressure, and ρ_m the material density.

The force given by the detonation can be obtained by the following equation:

$$F_t = ma = \pi R l t_p \rho \frac{{V_w}^2}{g}$$

Where F_t is the total force applied on the tube, m the mass, R the average radius of the external tube, the overlapping length of both tubes.

2.1.2. Magnetic pulse welding (MPW)

Magnetic pulse welding is a recent technology in the field of impact welding. The principle of this process consists is on follows: two workpieces are placed into or around a coil with a gap in between to create the magnetic force necessary for welding.

The current passes through coil and thus create the magnetic fields around it (figure 7). This magnetic field leads to the apparition of an induced current in the work-piece. This last creates a second magnetic field then the Lorentz forces observed from both sides repel each other. This results in a pressure of around several hundred MPa on the flyer plate which propels it against the base plate.

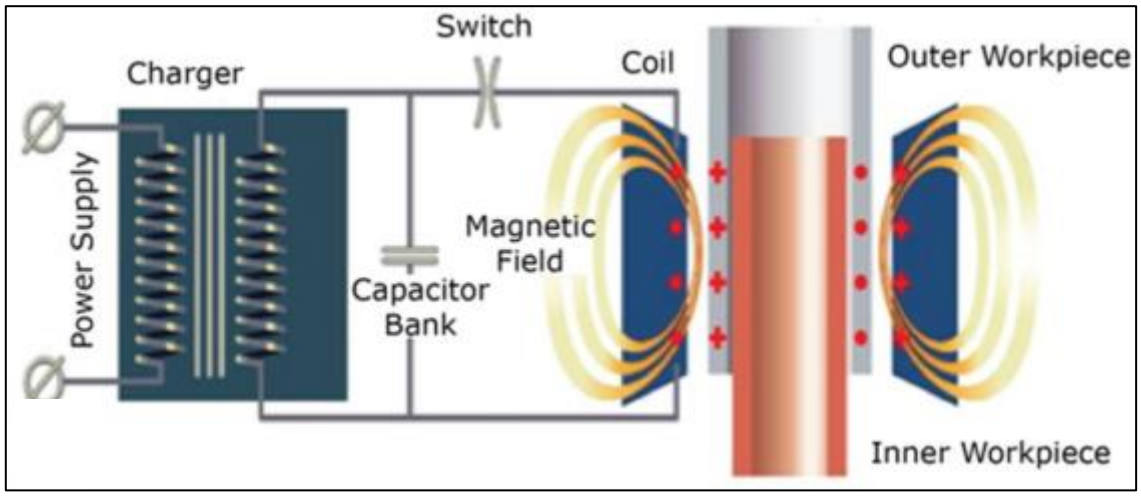

Figure 7. MPW principale [5]

There is no longer a detonation velocity, but a discharge of energy E_d defined by the following expression (Where C is the capacitance and U the loading voltage)

$$E_d = \frac{CU^2}{2}$$

The frequency of the circuit f is written:

$$f = \frac{1}{2\pi\sqrt{LC}}$$

Where L is the inductance of the circuit.

The magnetic pressure P_m is defined as follows:

$$P_m = \frac{\mu_0 K^2 w^2 U^2 C sin^2\left(\left(\frac{1}{2\pi\sqrt{LC}}\right)t\right) exp\left(-\frac{rt}{L}\right)}{2L{I_w}^2}$$

Where μ_0 is the magnetic permeability, K is a constant depending of the geometry of the coil, w is the number of turns of the coil, I_w is the length of the coil working zone, r is the resistance of the discharge circuit.

The induced magnetic force F_m and the force induced by the resistance of the plates against deformation F_σ can be obtained with the following equation:

$$m_p \frac{d^2 g}{dt} = F_m - F_\sigma$$

Where m_p is the mass of the flyer plate.

2.1.3. Vaporizing Foil Actuator Welding (VFAW)

Vaporizing Foil Actuator Welding (figure 8) is a process in which a flyer is launched toward the base by pressure created from a electrical resistor standoff.

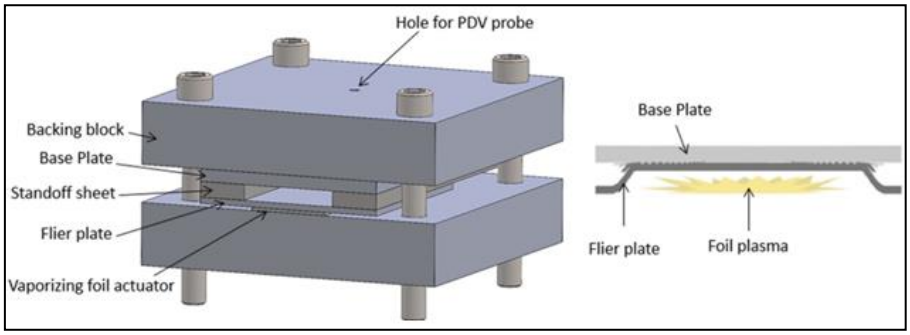

Figure 8. VAFW process [3]

These three processes belong all to the impact welding category. The difference consists in the source of the initial energy required to propel the flyer plate towards the fixed plate. In this different process, the physical phenomena related to joining mechanism are very similar and are introduced in the next section.

2.2. *Detail analysis of the welded interface and the related physical phenomena*

2.2.1. Interface

There are three types of interfaces according to the metallographic analysis: straight, wavy and vortical interface.

2.2.1.1. Straight interface

This type of interface, illustrated in figure 9, doesn't present any default. Both materials are stuck together without any microscopic interaction.

Figure 9. Microscopic of a straight weld interface [6]

2.2.1.2. Wavy interface

In this type of interface (figure 10), the wave is present with a regular frequency and amplitude. The value of these wave depends on the thickness, the initial energy instead and the materials used for the weld.

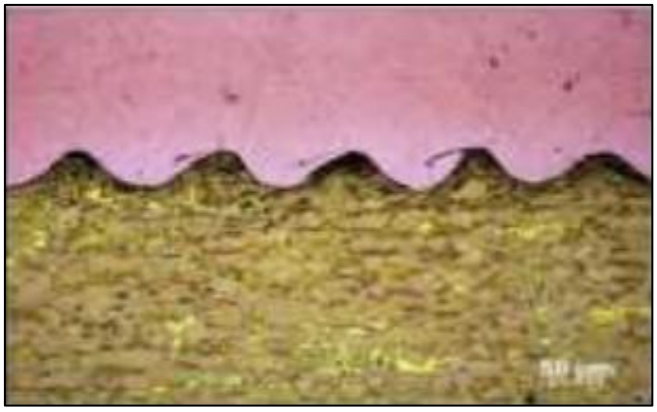

Figure 10. Microscopic of a wave weld interface [5]

2.2.1.3. Vortical interface

In this case, the welded joint presents a wavy interface with a vortex into the trough of each wave. The crest at the top the wave is created by the vortex.

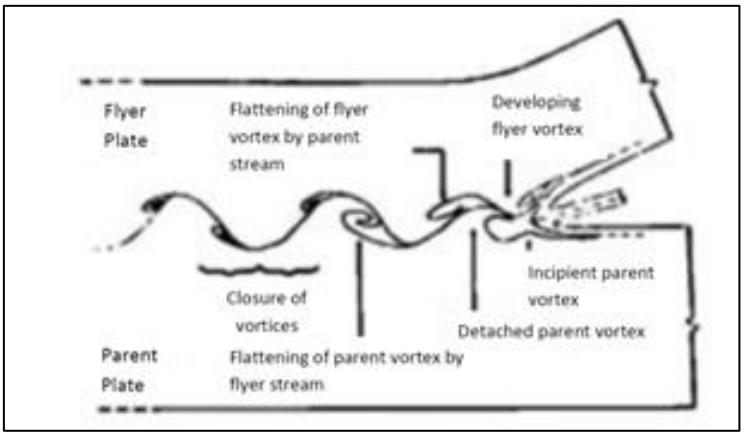

Figure 11. Schema of the vortex formation [6]

2.2.2. Jet

In impact welding, the pressure released during the weld creates a jet (figure 12) which composed on the base and the flyer materials and their densities. To understand well this phenomenon, Gallizzi [6], proposed the following scheme of flow to show the layer which are involved into the jetting. The impact cleans the superficial layer and the oxides, and these particles are forming the jet.

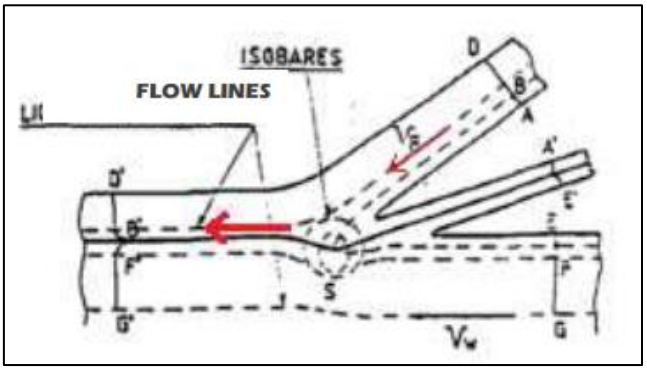

Figure 12. Scheme of flows explication of the jet formation [6]

2.2.3. Slug

The "slug" is the material that is deposited upstream of the welding point of collision. It moves slowly in the direction of the weld for an external observer but moves slowly to the opposite direction when this observer is placed at the stagnation point. The slug is composed by the material of the flyer plate only, although the jet is formed of the materials of the two plates Gallizzi [6] (figure 13).

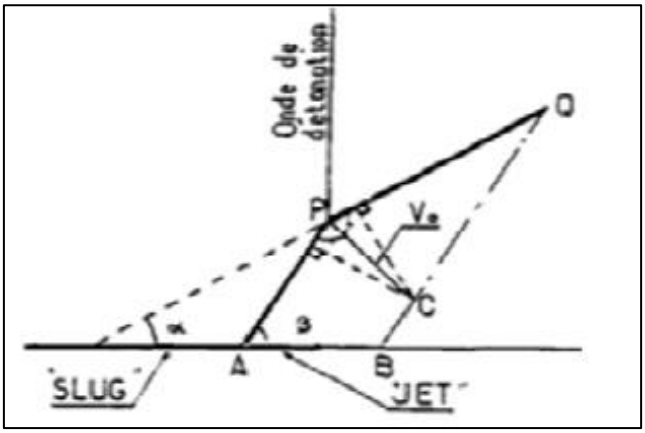

Figure 13. Scheme explaining the Slug's formation [6]

2.2.4. Hump

The collision between the two plates creates, downstream from the collision point, a hump by moving some material from the base plate toward the movable plate. This hump, illustrated in figure 14, appears in many theories as a cause of the formation of waves and vortices.

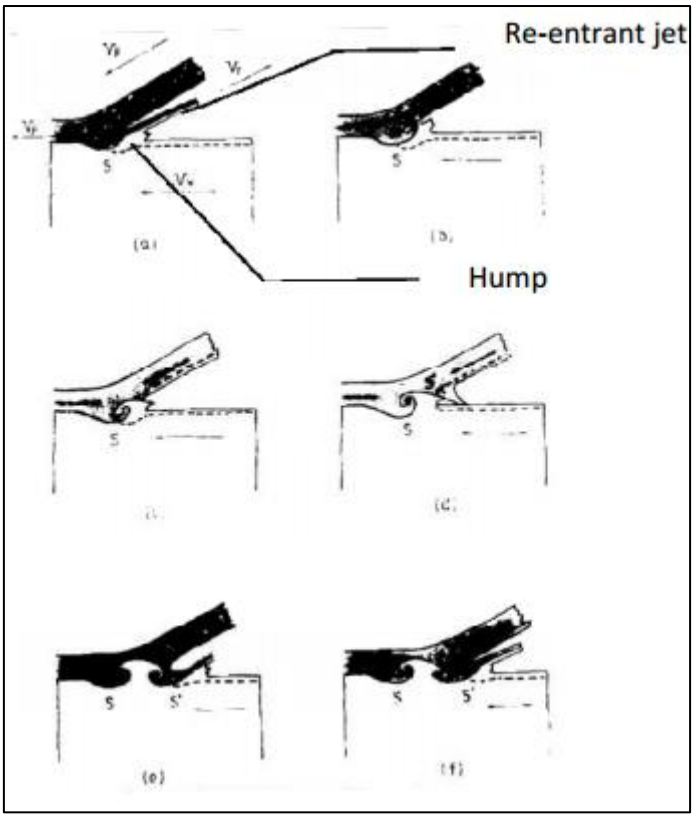

Figure 14. Apparition scheme of the hump, and its purpose in the wave formation [6]

2.3. *Fusion welding*

Fusion welding, illustrated in figure 15, is a process where the joint is created by localized heating of the edges of the base metals, above their melting temperature. A filler metal may or not be used and no external pressure is required. Inter gases may or may not be used to enhance the quality of the weld created. The welded joint is achieved after solidification of the fused pool with a metal which must possess some degree of mutual solubility in solid state. Two types of metal are present: Metals that are completely soluble in the solid state, exhibit the highest degree of weldability, and the second type is metals with no solubility in solid state which are not weldable, for which an intermediate soluble metal is used.

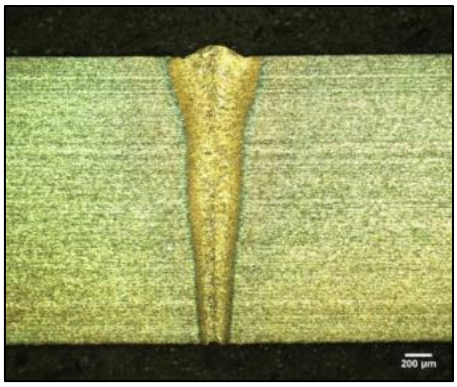

Figure 15. Fusion welding [7]

As it is mentioned in figure 4, many types of fusion welding exist. Some of them are introduced in the next sections.

2.3.1. Electric arc welding

The arc welding (figure 16) is one of the most common for which the heat required to fuse the metal is obtained from an electric arc between the base metal and an electrode.

The electric arc is produced when two conductors are touching together and then are separated by a small gap of 2 to 4 mm, such that the current continues to flow through the air. The temperature produced by the electric arc is about 4000°C to 6000°C.

An electric current, in the form of the either alternating current (A.C) or direct current (D.C) from a welding power supply, is used to from an electric arc between the electrode and the metals to be joined.

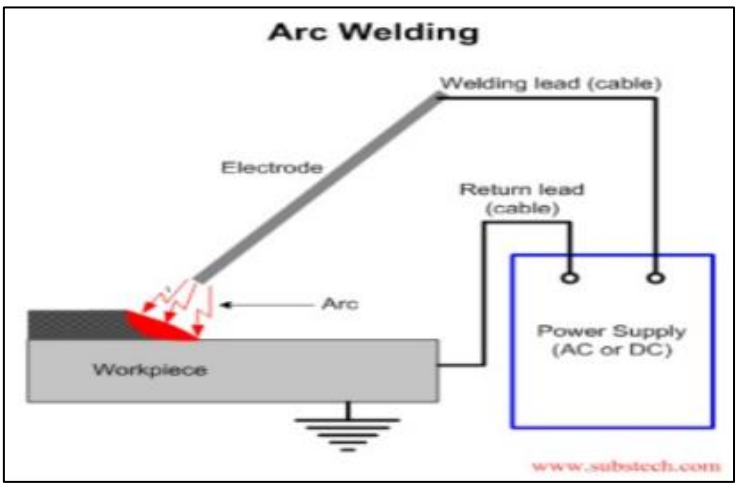

Figure 16. Electric arc welding [8]

The alternating current for arc is obtained from a step-down transformer. The transformer receives current from the main supply at 220 to 440 volts and steps down to required voltage i.e., 80 to 100 volts.

The electric arc welding goes through several steps: first, the work piece should be cleaned in order to remove the grease, oil, … Secondly, a suitable electrode is inserted in the electrode holder at an angle of 60 to 80 degree with the workpiece. After that, the welding is done by making contact of the electrode with the workpiece and then the electrode is fixed to a proper distance to produce an arc. Then, the arc being obtained, an intense heat is produced which melts the workpiece below the arc and forms a molten metal pool. Finally, after the welding is over, the electrode holder should be taken out quickly to break the arc and the supply of current is switched off.

In this process, many process exist such as MIG, MAG, TIG, Submerged arc, etc.

2.3.1.1. Gaz Metal Arc Welding (GMAW)

GMAW is suitable for welding a variety of ferrous and nonferrous materials.

The coalescence of the workpieces is produced by heating them with an arc which melts the wire as it is fed in the weld puddle. The weld area is shielded by a flow of gas and the consumable bare wire is fed automatically.

Different categories exist depending on the type of gas. For example, the well know Metal Inert Gas (MIG), illustrate in figure 17.

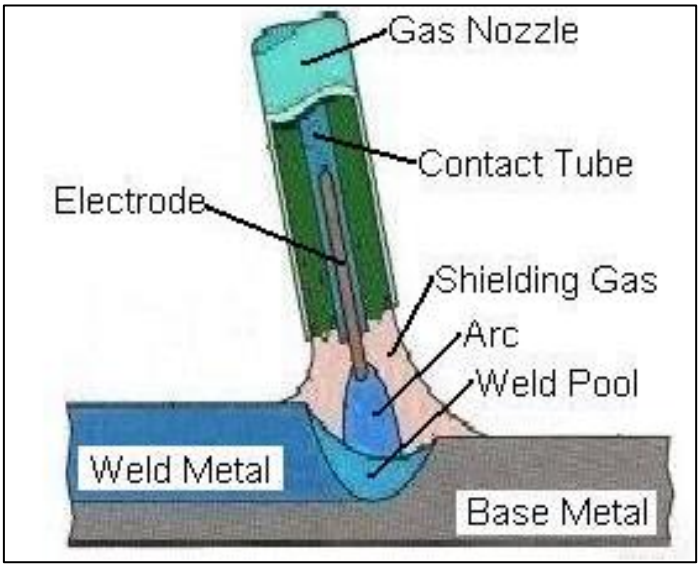

Figure 17. MIG process [9]

2.3.1.2. Gas Tungsten Arc Welding (GTAW)

Gas Tungsten Arc Welding called also Tungsten Inert Gas (TIG) is illustrated in figure 18. This process uses heat generated by an electric arc struck between a non-consumable tungsten electrode and the workpiece to fuse metal and filer wire in the joint area and produce a molten weld pool.

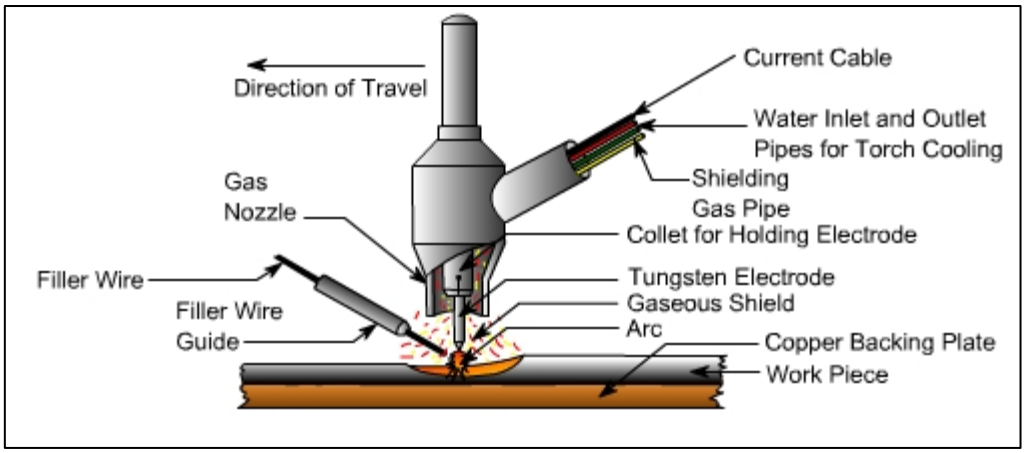

Figure 18. TIG principal [10]

2.3.1.3. Submerged arc welding (SAW)

SAW is illustrated in figure 19. It is a process in which welding is done by an automatic electrode feeding machine wherein the tip of the electrode is submerged into a granular flux which shields the arc and the molten metal. SAW is safer than other process in fact: the arc is completely covered during welding hence the term submerged arc.

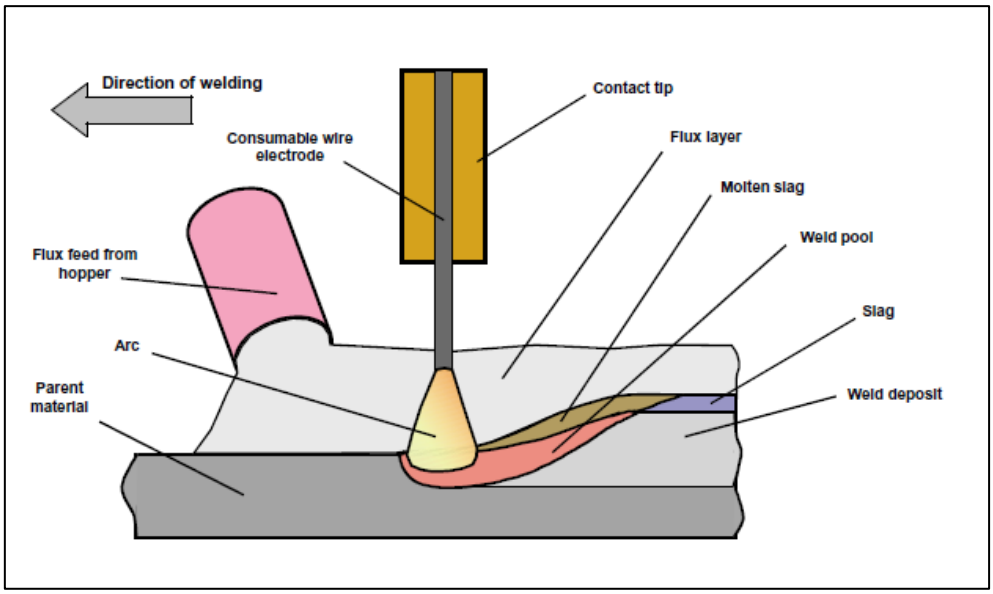

Figure 19. SAW principle [11]

2.3.2. Electric resistance welding

Electric resistance welding belongs to a fusion welding category. It is a thermo-electric process in which the heat is generated at the interface of the parts to be joined. An electric current follows through the parts under a controlled time and a controlled pressure. It has different variants such as seam welding, projection welding and spot welding.

2.3.2.1. Seam welding

In seam welding (figure 20), overlapping sheets are gripped between two electrodes (roller). These wheels roll over the metal, and the current is conducted through the metal from the wheel on one side to the wheel on the other side. Heat caused by the current flowing through the resistance of the metal softens the metal, and pressure between the wheels forces the softened metal in the two pieces to join together.

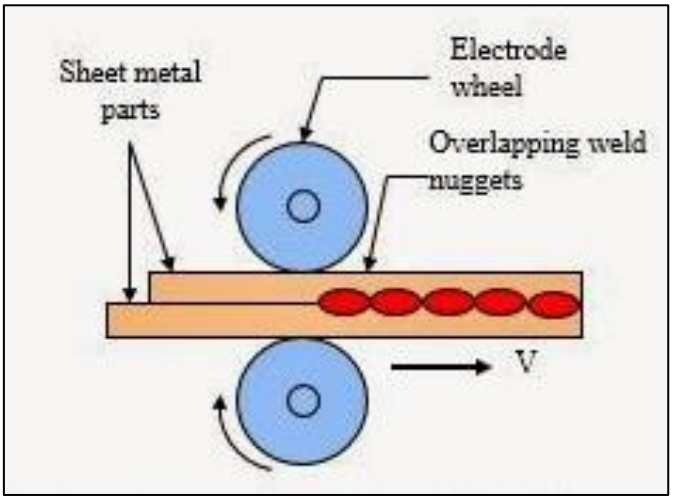

Figure 20. Seam welding principle [12]

2.3.2.2. Spot welding

Spot welding, illustrated in figure 21, is a method of electric resistance welding. It is a method of welding uses two sheets of metal which are clamped and assembled between the electrodes. It uses shaped copper alloy electrodes to apply pressure and convey the electrical current through the workpieces. The material between the electrodes yields and is squeezed together. It then melts, destroying the interface between the parts. The current is switched off and the "nugget" of molten materials solidifies forming the joint.

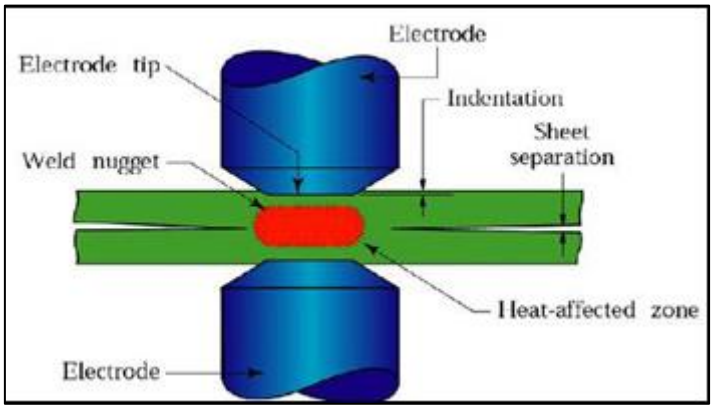

Figure 21. Spot welding principle [12]

2.3.3. Gas Flame Welding

Gas Flame Welding, illustrated in figure 22, also known as Oxy-Acetylene welding process uses acetylene as fuel. In this process, the filler metals are used to bring additional material to the weld zone during welding. They are available as rod or wire, coated and uncoated, and are made of metals compatible with those to be welded. Oxyacetylene welding can be used with most ferrous and nonferrous metals for any thickness of workpieces, but the relatively low heat input limits the process economically to less than 6 mm. A variety of joints can be produced by this method.

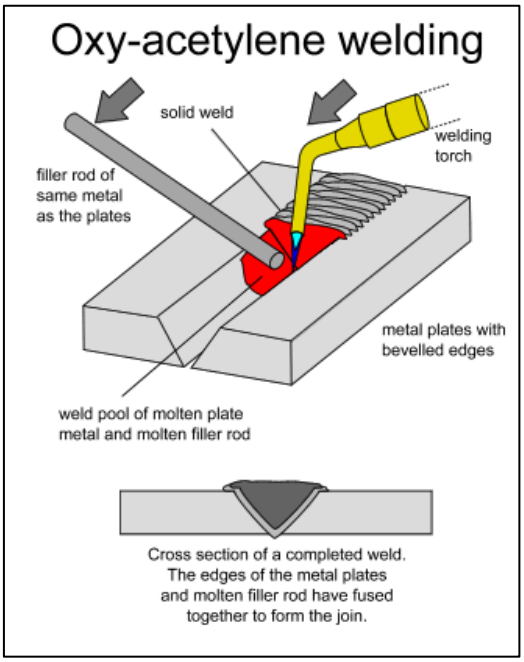

Figure 22. Oxy-acetylene Welding [13]

3. Computational welding mechanics

3.1. *Introduction*

Experimental testing is costly and time consuming. To avoid this, Numerical simulations could be used to evaluate the quality of a weld. Numerical modeling can simulate the whole welding process, predict its behavior and optimize it. To validate numerical procedure, the experience remains essential. The Finite element method is used most of the time to simulate welding processes (figure 23).

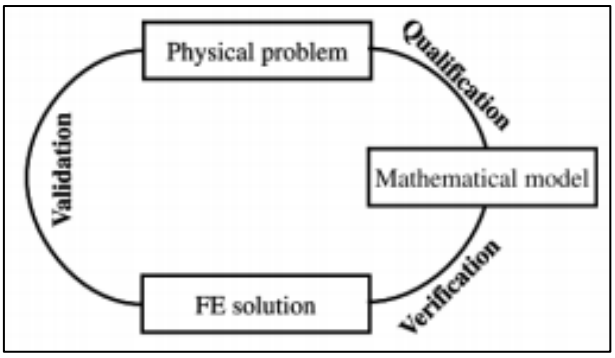

Figure 23. Validation of finite element modeling [14]

3.2. *Computational welding mechanics*

The overall aim of computational welding mechanics (CWM) is 'to establish methods and models that are usable for control and design of welding processes to obtain appropriate mechanical performance' [14]. Many phenomena exist in the welding process. These phenomena can be divided in different fields is shown in figure 24 where the box 'physics of heat generation' is generic presentation for all possible welding process.

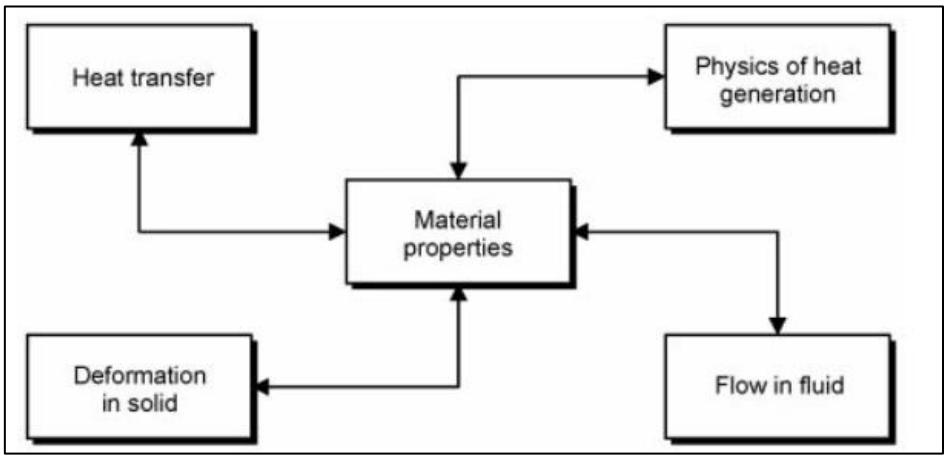

Figure 24. Different field in CWM modeling [14]

In CWM, it has been possible to decouple the modeling from the physics of the welding process. And most analyses in CWM ignore the 'Flow in fluid' and prescribe the distribution of the 'Heat input model' as shown in figure 25.

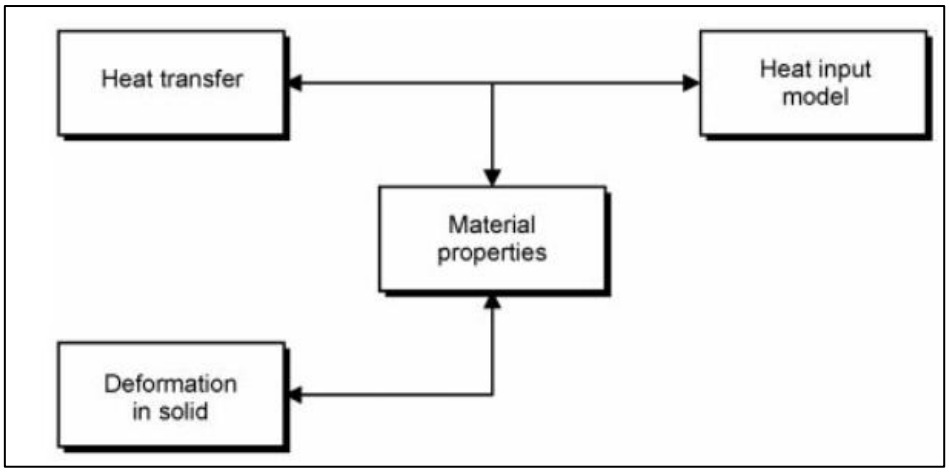

Figure 25. Fields in classical CWM modelling of fusion welding without a welding process model and without fluid flow [14]

This coupling poses some problems (in some approach the mechanical fields generate heat). This probably because the coupling term is small and the demand for accuracy limits the time step used. To solve this problem, researchers found a solution: the use of monolithic approach. And the coupling between material behavior and the temperature and deformation fields is shown in figure 26 and explained in table 2.

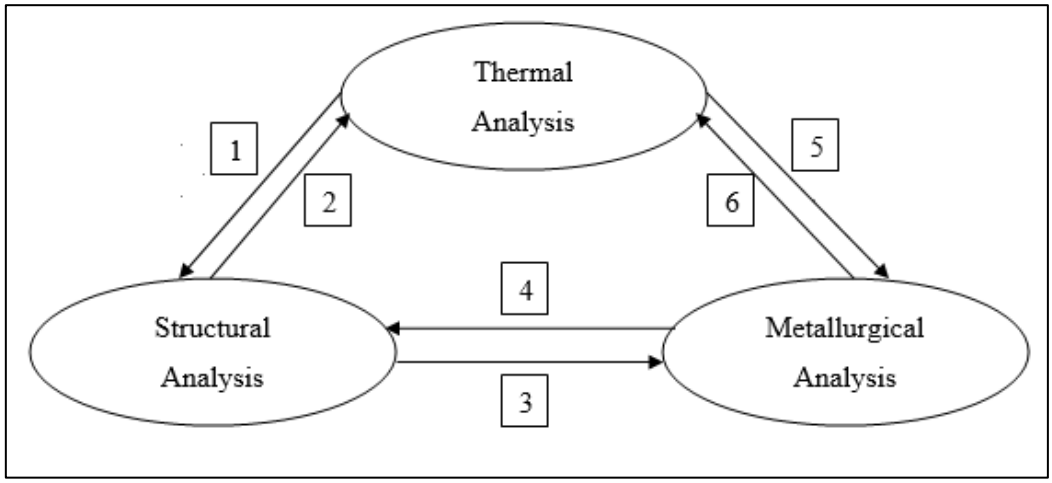

Figure 26. Couplings between the different Analysis [14]

Table 2. Couplings in figure 26 [14]

1	Thermal dilatation drives the deformation.
2	Deformation generates heat in material due to plastic energy dissipation.
3	Deformation affects the microstructure changes.
4	Mechanical properties depend on microstructure and temperature.

5	Temperature drives the microstructure changes.
6	Thermal properties depend on microstructure and phase changes

According to the literature, couplings 4 and 6 are negligible.

The goal of modeling is to retain the essential features of the problem. To achieve this goal, there is always some reduction of the accuracy of the results. So, a modelling strategy is needed. Many aspects are present in the welding modelling. The most critical are: the heat input model, the material model and the geometric model together with a discretization issue (figure 27).

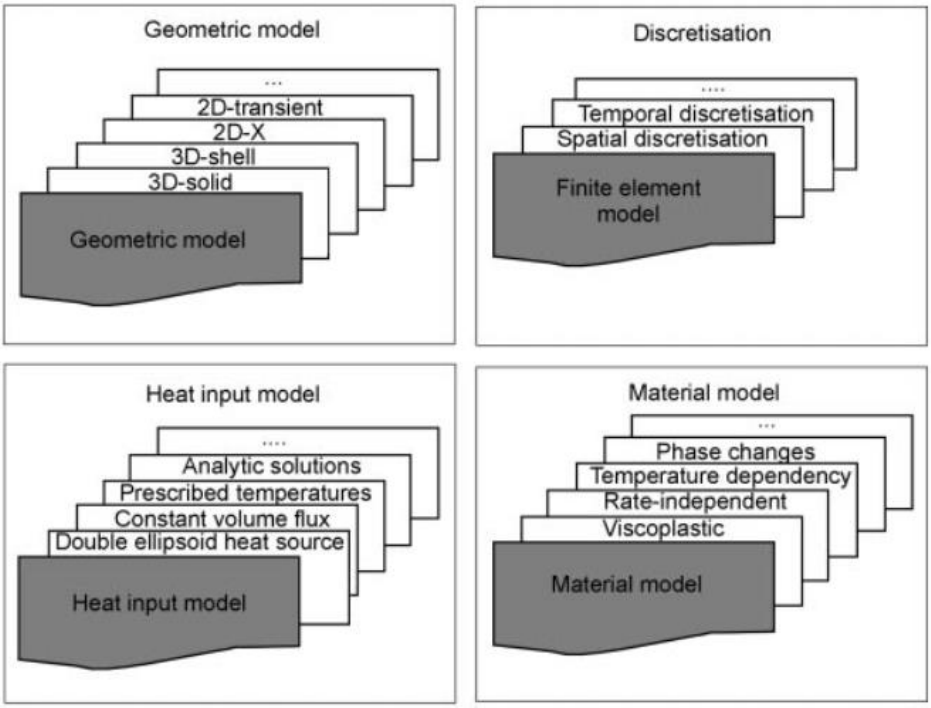

Figure 27. Different sub-models for the accuracy of CWM models [14]

The accuracy depends on the model chosen and the values of the associated parameters. To choose the accuracy, we should answer the question "What is question to be answered by the simulation". Therefore, the different accuracy categories are defined in figure 28.

Simulation accuracy	Computation objectives
Reduced accuracy level simulation	Simple, fast models
Basic simulation	Calculation of residual stress and distortion for simple geometries Neglect of the material behaviour in the high-temperature range
Standard simulation	Calculation of residual stress and deformation for complex geometries Calculation of transient stress and deformation
Accurate simulation	Calculation of residual stress and deformation for complex geometries taking account of the microstructure
Very accurate simulation	Extended detailed simulation, e.g. hot cracking

Figure 28. Accuracy levels wanted in a welding simulation [15]

4. Conclusion

The aim of this chapter is to introduce welding in order to understand the project. This chapter contain different parts: CWM with the different coupling present in thermomechanical welding and two types of welding (impact and fusion) where the studies are present in the next chapters.

Chapter 3:

Impact welding

1. Introduction

An impact welding is a process in which the pressure is applied to produce the welding joint with a temperature below the melting point. In this chapter, we studied 2 cases: Nassiri case [3] in order to compare our simulation with his results and Join'EM cases.

For both study, the finite element software from MSC corporation (Marc as solver and Mentat as post-processor) have been used. A thermo-mechanical simulation with the equations to be solved by FEA are:

- Mechanical Analysis

$$\nabla\sigma + \vec{f}_{int} = \rho \frac{\partial^2 u}{\partial^2 t}$$

$$\sigma = C\varepsilon^e$$

$$\varepsilon = \varepsilon^e + \varepsilon^p + \varepsilon^{th} \text{ with } \begin{cases} \varepsilon^e = \frac{1+\upsilon}{E}\sigma - \frac{\upsilon}{E}\, tr(\sigma)\mathbb{I} \\ \varepsilon^p = g(\sigma_y) \\ \varepsilon^{th} = \alpha\,(\theta - \theta_0) \end{cases}$$

- Thermal Analysis

$$\rho \frac{dh}{dt} = \nabla(\lambda \nabla T) + Q_v$$

The unit's system used is mm/tonne/s/K.

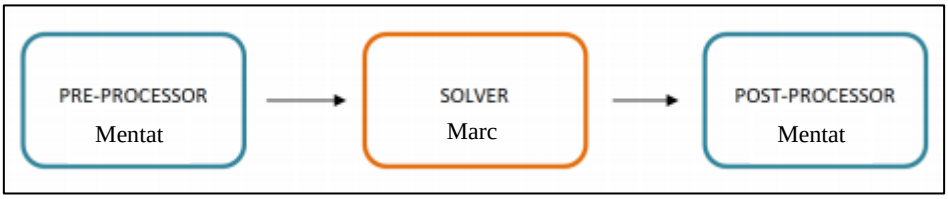

Figure 29. Flowchart of the numerical simulation chain

2. Nassiri case study

The aims of this study, is to compare our numerical results with Nassiri [3] results in order to validate our numerical methodology. For that, we take the same model as Nassiri [3]. The model and the results are presented in the following section.

2.1. *Model description*

The base model chosen for this simulation carried out is Nassiri [3] case. Because of its simplicity, it was chosen amongst of many studied articles. The geometry, the material, the boundary condition, the initial condition, etc, are given in more detail in the next section.

2.1.1. Geometry / Mesh

Due to the configuration, 2D assumption has been made. The geometry is made up of a base plate and a flyer plate whose dimensions 15 mm by 3mm and 12mm by 2mm and with an impact angle $\alpha = 7°$ between them.

The initial mesh is made up of linear quad element of 2D plane strain type. Three Regions are defined, illustrated in figure 30, for the mesh in fact: a finest mesh is located near the interface (Region A), an intermediate mesh in the middle (Region B) a larger mesh is defined on the outer-most part of the plates (Region C).

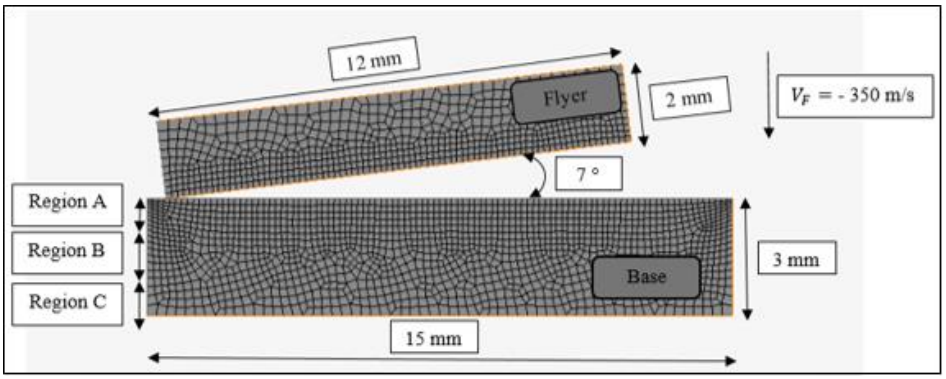

Figure 30. FEA model with varying mesh densities in three regions (Nassiri geometry)

A global re-meshing procedure is used, figure 31, that is the mesh is evolving over time. To capture gradients near the interface, 2 boxes for the refinement region for both base and flyer are defined. The number of element increases from 2159 to 19065 and at the end, we have Minimum Edge Length (MEL) value of 20 μm coarsening can occur if detected.

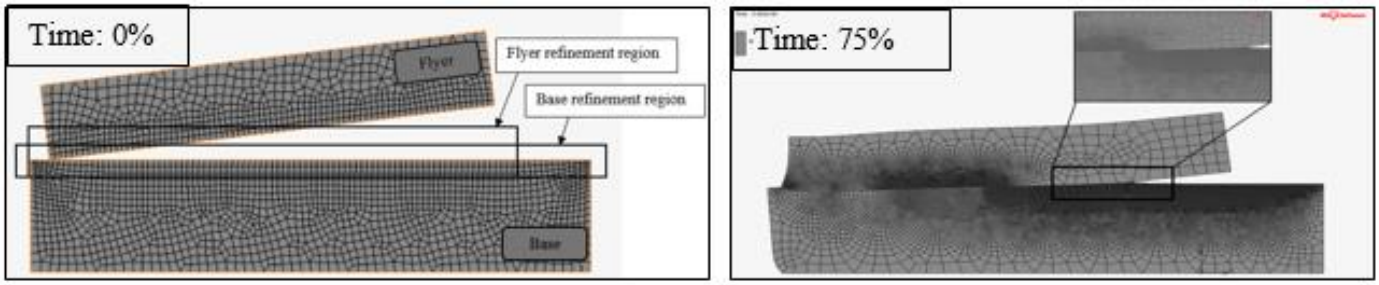

Figure 31. a) Initial mesh b) Mesh at 75% of the time

2.1.2. Material proprieties

For Nassiri case [3], we used Al6061-T6 aluminum for both base and flyer whose characteristics are illustrate in table 3. The flow rule is the well-known Johnson-Cook constitute law:

$$\sigma_y = (A + B{\varepsilon_p}^n)(1 + Cln\dot{\varepsilon_p})(1 - T^{*m})$$

Where σ_y is the follow stress (the yield criterion is Von Mises), ε_p is the plastic strain, $T^* = \frac{T - T_{room}}{T_{melt} - T_{room}}$ is the homologous temperature (at the melt temperature T^* =1) and A, B, C, n and m are material parameters.

Table 3. The material properties for Al6061-T6 and the Johnson-Cook model parameters [3]

ρ (kg/m^3)	E (GPa)	υ	k (W/mk)	C (J/kg°C)
2700	70	0,279	154	860

A (MPa)	B (MPa)	C	n	m	ε_0	T_{melt} (°C)	T_{room} (°C)
289	108	0,011	0,42	1,34	1	653	23

2.1.3. Initial and boundary conditions

- Initial conditions

Two initial conditions are present: a vertical velocity value of -350 m/s imposed on the flyer and a fixed temperature of 296 K fixed for both the flyer and the base. Both initial conditions are presented in figure 32.

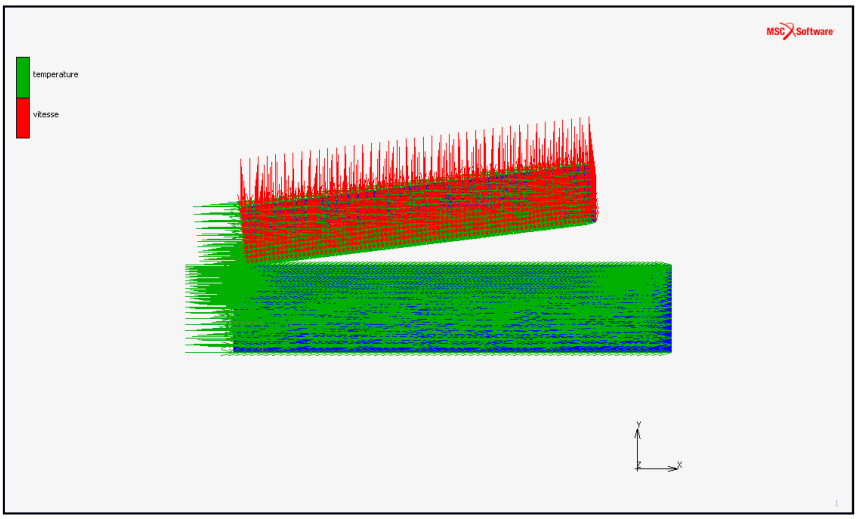

Figure 32. Initial conditions

- Boundary conditions

A null displacement fixed at the bottom of the base and a vertical gravity load for both the base and the flyer are imposed. The structural conditions are illustrated in figure 33.

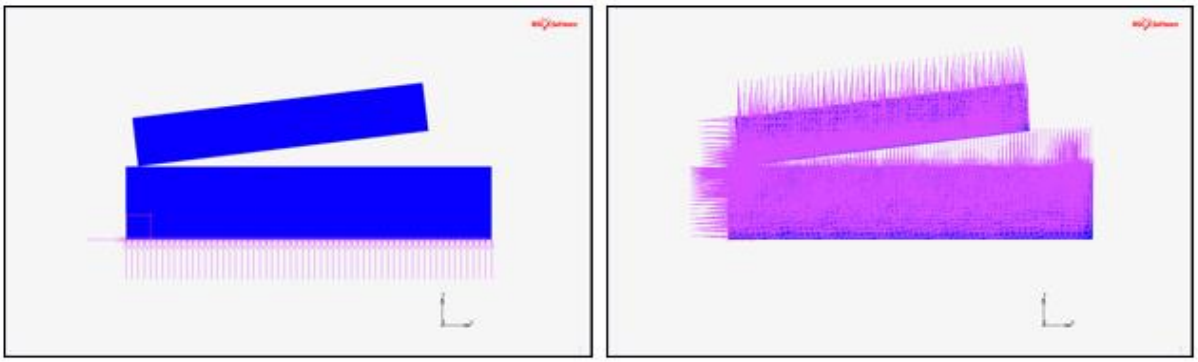

Figure 33. Structural conditions: a) fixed displacement b) gravity load

A fixed temperature of 296 K is imposed at the bottom of the base. A plastic heat generation for both the base and the flyer (Correction factor of 0,9) is imposed and an adiabatic condition is considered (only conduction is considered here due to the rapidity of the process order of few μs). The thermal conditions are illustrated in figure 34.

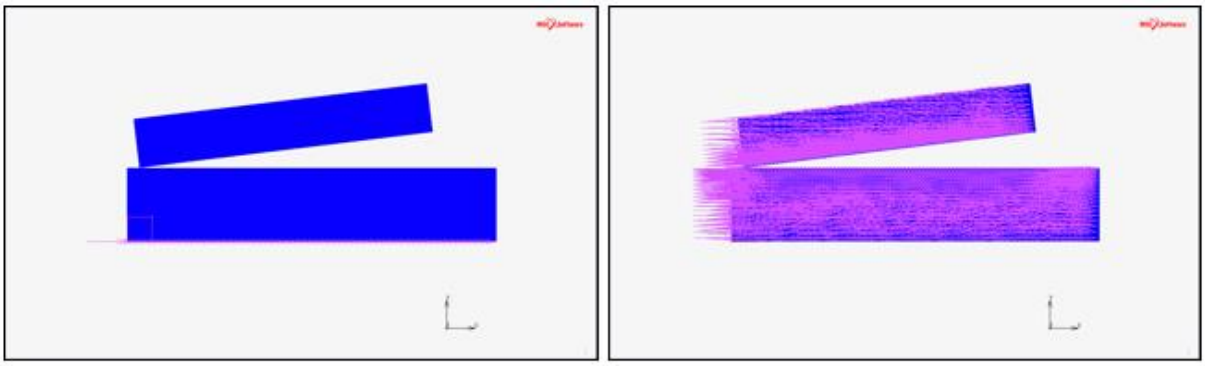

Figure 34. Thermal conditions: a) fixed Temperature b) plastic Heat Generation

2.2. Results

2.2.1. Effective Plastic Strain

The figure 36 shows the behavior of our model at 1 μs , 2.5 μs and 4 μs. It is increase from 0.9 to 1.6 at 1 μs and 2.5 μsrespectively and decrease after that to 1 at 4 μs. The annealing effect isn't considered.

According to the SERIZAWA & al [16], two types of plastic distribution are obtained by varying the collision velocity and the collision angle. These two types are illustrated in figure 35 and the effect of the collision velocity and the collision angle is illustrated in table 4.

In our case the value of the angle is 7° and the collision velocity is 350 m/s (we are in the case pattern B). The figure 8 shows that our results are comparable to the literature.

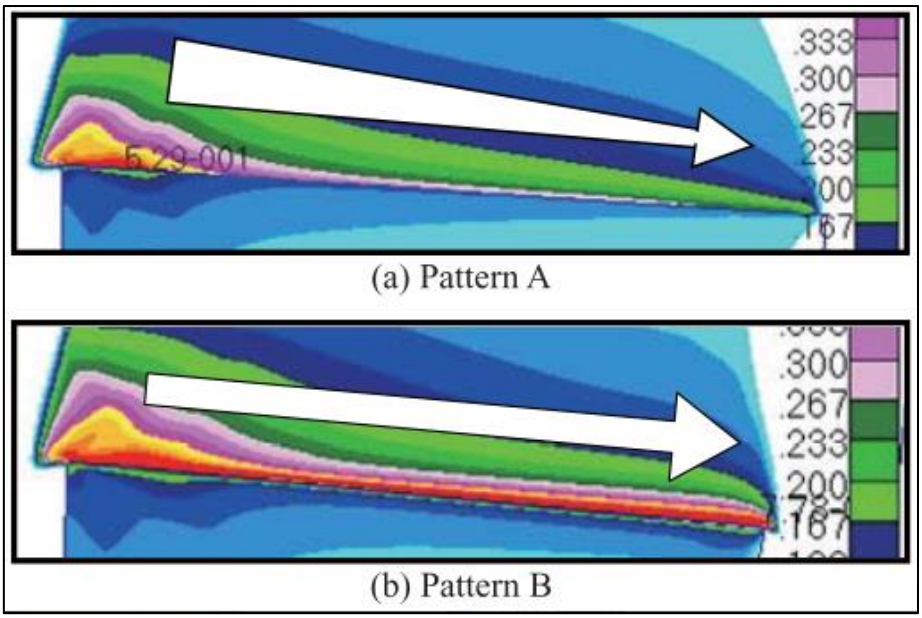

Figure 35. Plastic strain distribution near joint interface [16]

Table 4. Effect of collision velocity and collision angle on pattern of plastic strain distribution [16]

Collision Angle	Collision Velocity			
	100 m/s	200 m/s	300 m/s	500 m/s
0.5 degree	A	A	A	A
1 degree	A	A	A	A
2 degree	B	A	A	A
3 degree	B	B	A	A
5 degree	B	B	B	A
7 degree	-	B	B	B
10 degree	-	-	B	B

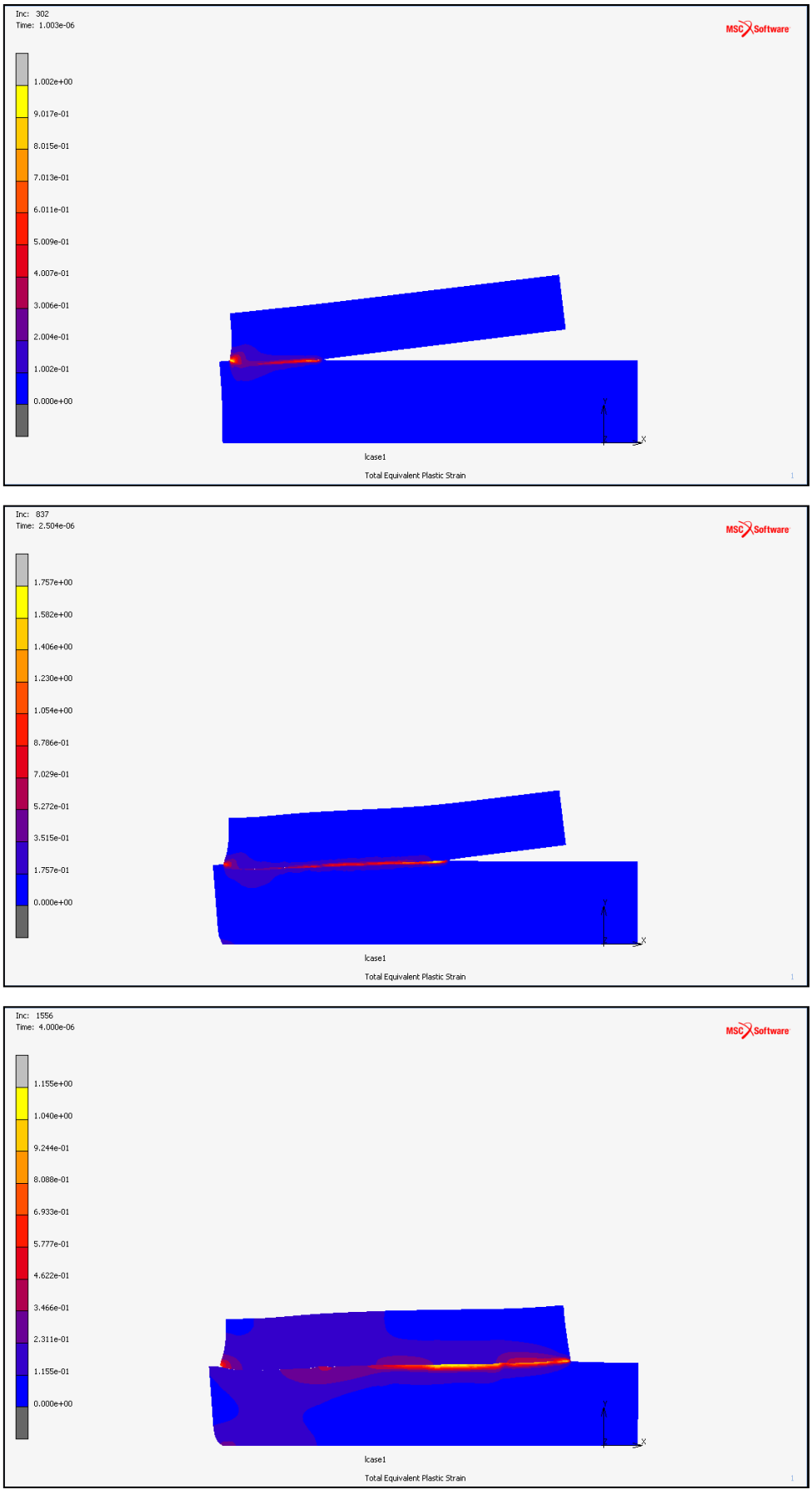

Figure 36. Effective Plastic Strain at 1 μs, 2.5 μs and 4 μs

2.2.2. Temperature

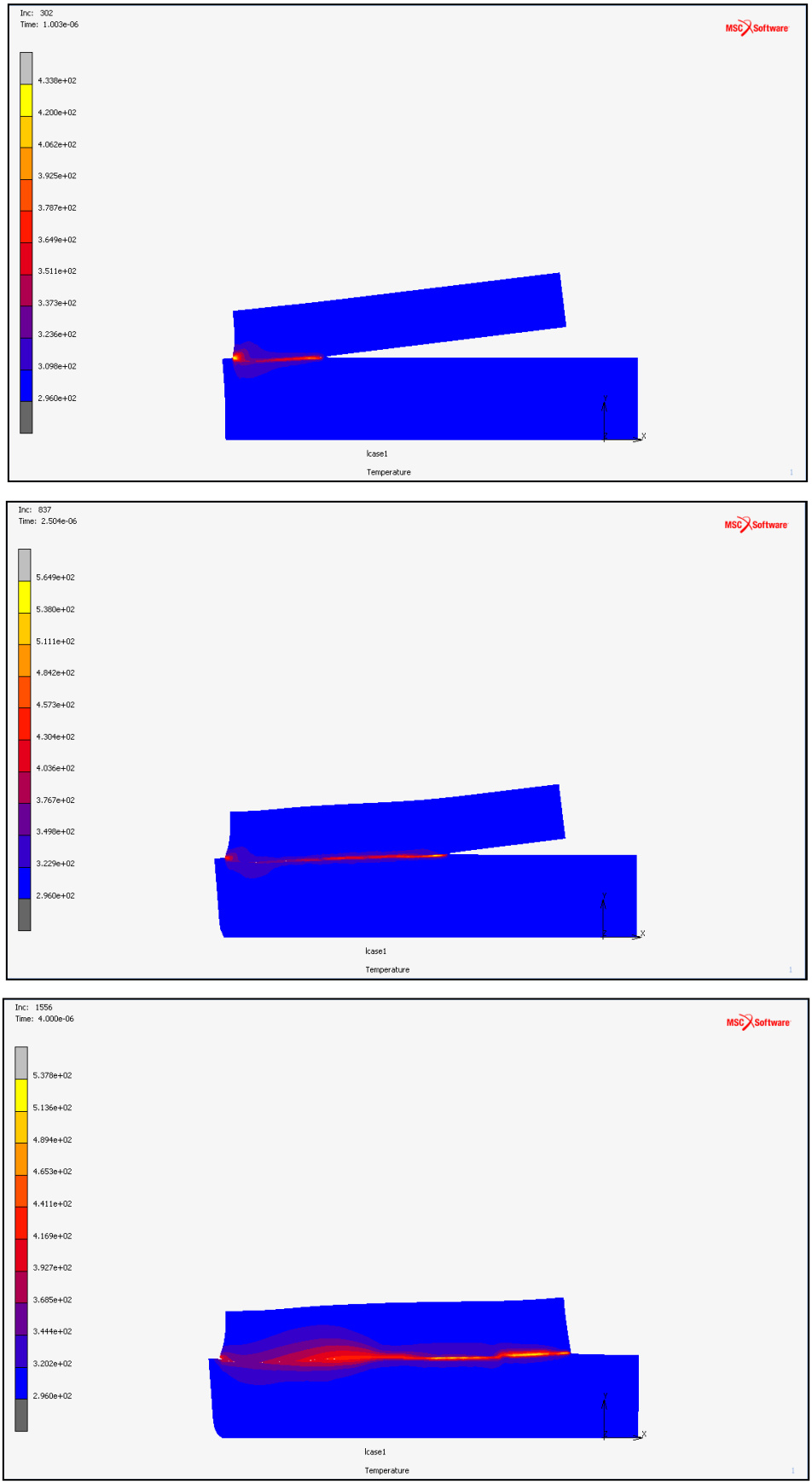

Figure 37. Temperature at 1 μs, 2.5 μs and 4 μs

The figure 37 shows the temperature behavior of our model: it rises from 420 K to 530 K at 1 μs and 2.5 μs respectively. And then, these later decreases 510 K at 4 μs.

To compare with Nassiri (see figure 38), the temperature at the end of the simulation is 700 K for our model and 900 K in his case. This difference is due of a Minimum Edge Length difference (in our model the MEL value is 20 μm, in Nassiri is 5 μm) which explain that in our case, we could not capture the very high temperature gradients.

The value of the maximum temperature is in the order of 700 which is below the fusion temperature of the Aluminum (926 K). Thus, the bonding was presumed to be a solid-state weld.

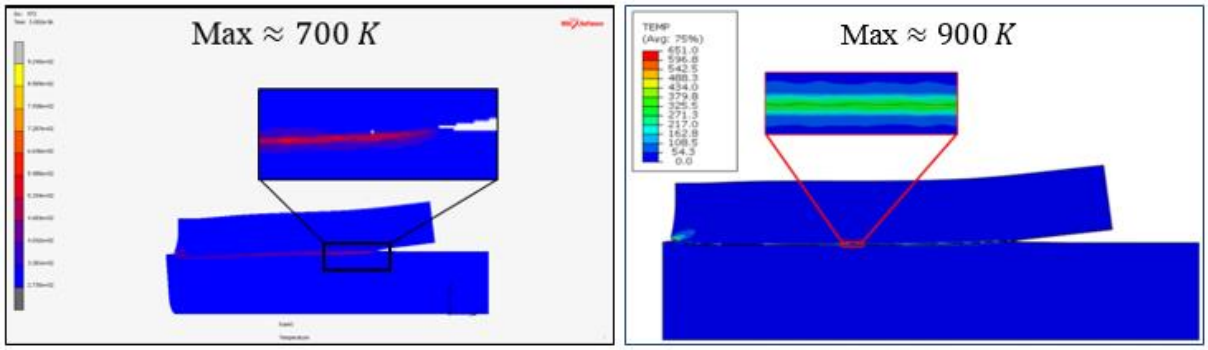

Figure 38. Comparison of the temperature between a) our model and b) Nassiri model

2.2.3. Impact angle

Along the welding, the impact angle increases from 7° (initial impact angle) to 14° at 3 µs. And then, it decreases to 0°. The evaluation of the value is similar to Nassiri's results [3]. The evolution of the impact angle is shown in figure 39.

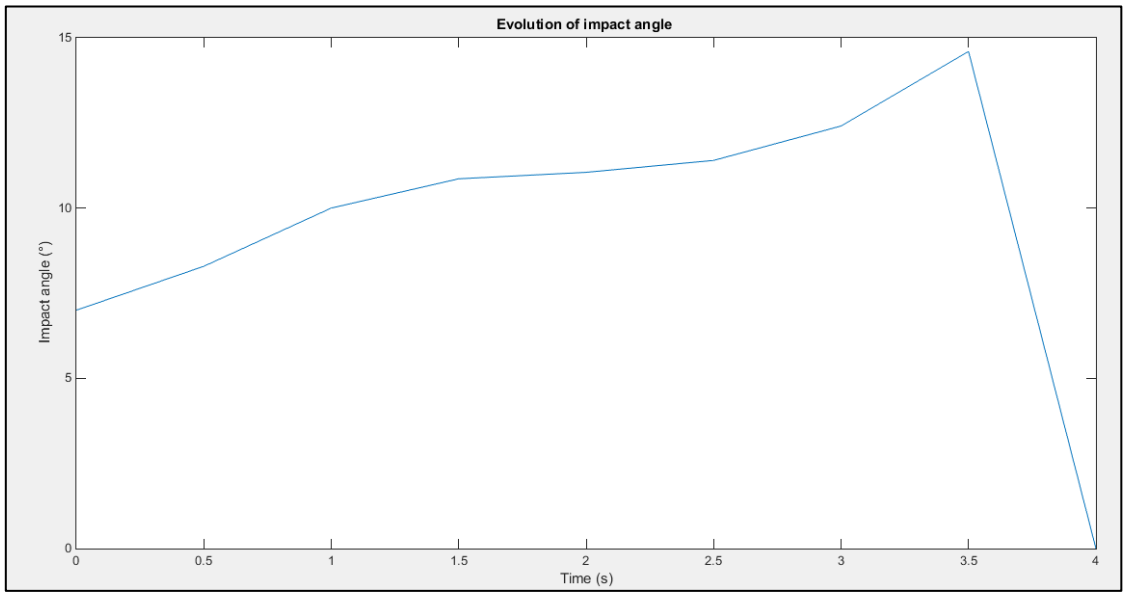

Figure 39. Evolution of impact angle

Nassiri's results are shown in figure 40 which are similar to ours.

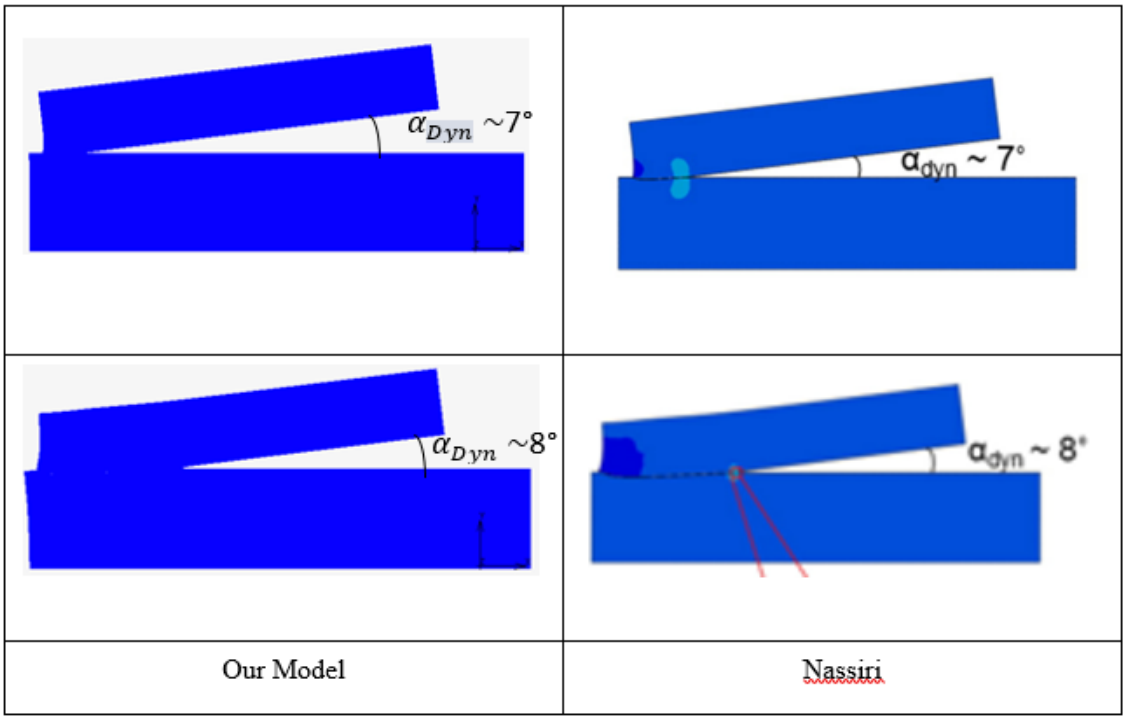

Figure 40. Comparison of impact angle

2.2.4. Velocity

The highest velocity occurs at the collision point. The behavior of the velocity is shown in figure 41. The value of the velocity also increases from 600 m/s to 1400 m/s between 1 μs and 2.5 μs and at 4 μs, it decreases to 1100 m/s. The experiences state that the welding velocity must be more than three times the initial velocity. Nassiri gave a weldability window which establishes the formation of a weld for a welding velocity higher than 1000 m/s.

To compare this value with Nassiri's article, as shown in figure 13, at 75% of the time, we find nearly 1400 m/s or Nassiri found 2200 m/s (figure 52). This difference is the result of the difference in MEL (20μm vs 5 μm).

To verify our result with the theory, assuming rigid body motion, with referring to the literature [17], the following equation used is:

$$V_w = \frac{V_p}{\tan \alpha}$$

Using this equation, the velocity could reach 2850 m/s which is much higher than the results given by the experiences and the simulations. This equation uses the incidence angle and by replacing it with the dynamic angle, we find a value closer to our simulations. We can criticize

this equation, which is disturbed because of the non-linear behavior at high strain rates according to Nassiri. But we compare the results to the given relation, using the Reynolds number [3]:

$$Vc = \sqrt{\frac{2Re_{transition}(H_{flier} + H_{base})}{(\rho_{flier} + \rho_{base})}} \sim 1400\ m/s$$

We obtain 1400 m.s-1 and it is in accordance to our simulations.

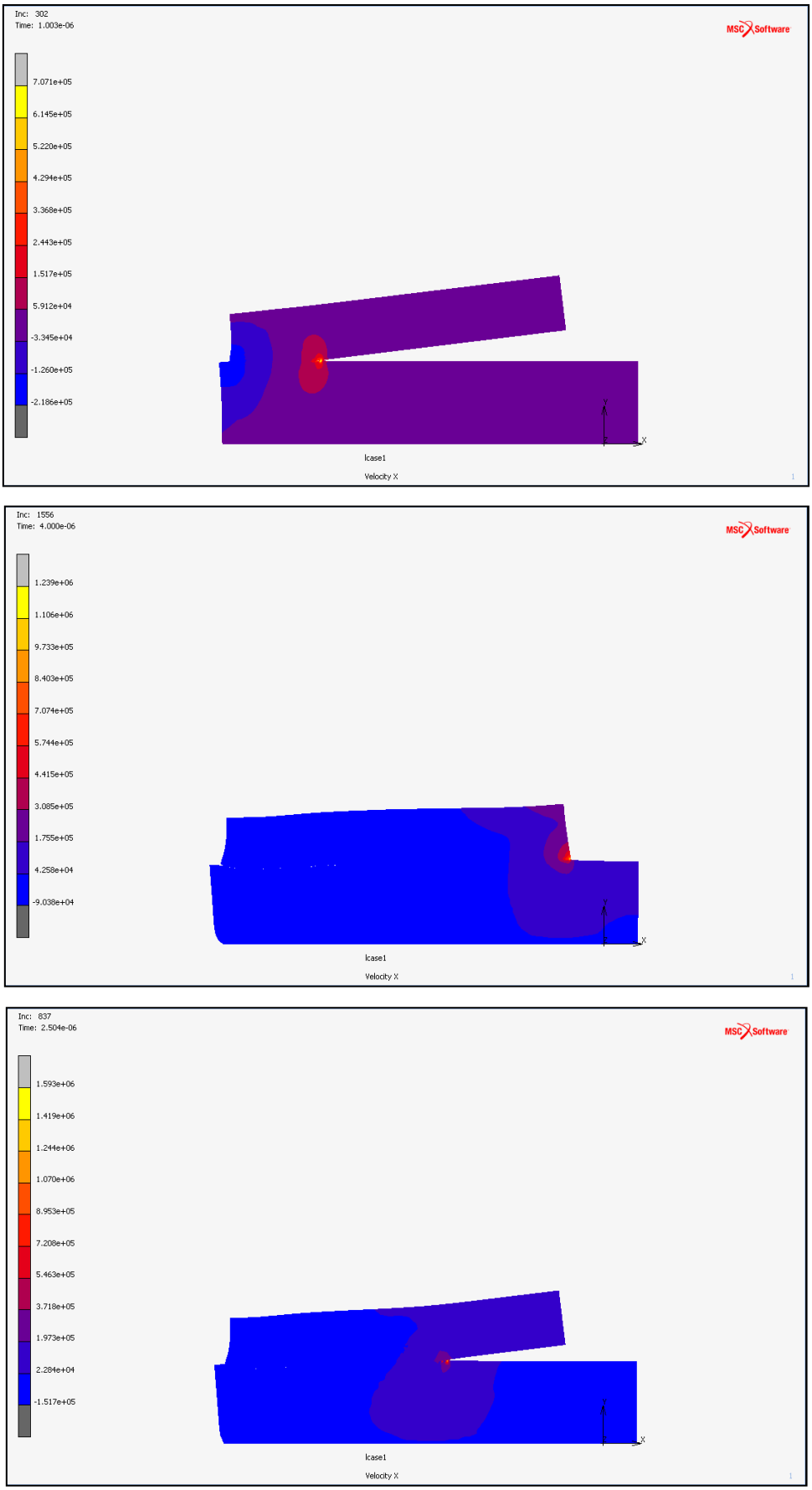

Figure 41. Velocity at 1 μs, 2.5 μs and 4 μs

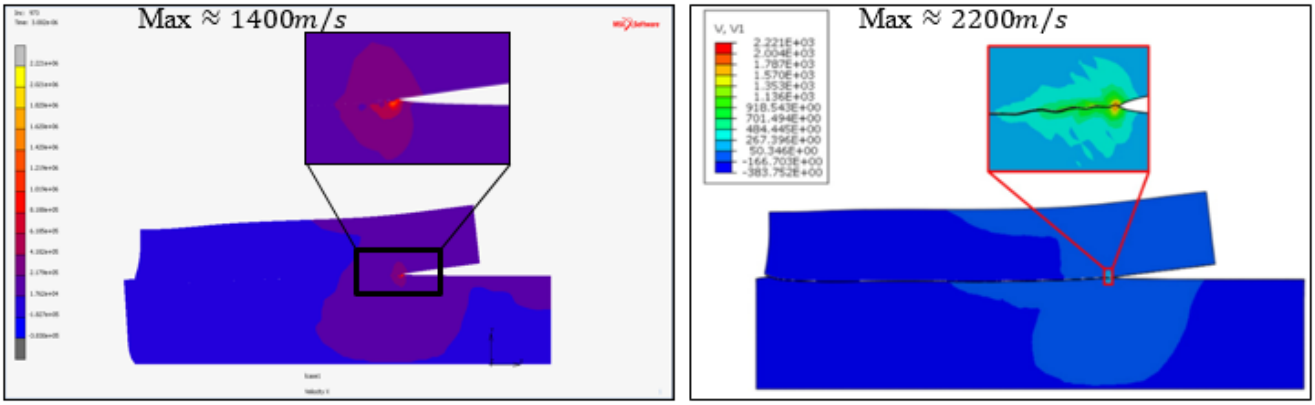

Figure 42. Comparison of the velocity between a) our model and b) Nassiri model

The time of simulation is calculated through the equation [17]:

$$t = \frac{2g}{V_w}$$

For the initial gap between the two plates, we obtain 1 μs as the duration of the process, to be compared the total duration of our simulation which is 4 μs. The order of magnitude is respected.

2.2.5. Pressure

The figure 43 shows that the highest pressure is at the collision point. This latter also increases between 1 μs and 2.5 μs from 3 GPa to 6 GPa and decrease after that to 3 GPa. This variation is logical in fact that the equation for the pressure depends on the velocity.

$$P_c = \frac{\rho_m {V_w}^2}{2}$$

Theoretically, we obtain 10 GPa which is higher than our result but we are at the same magnitude and our result are encouraging.

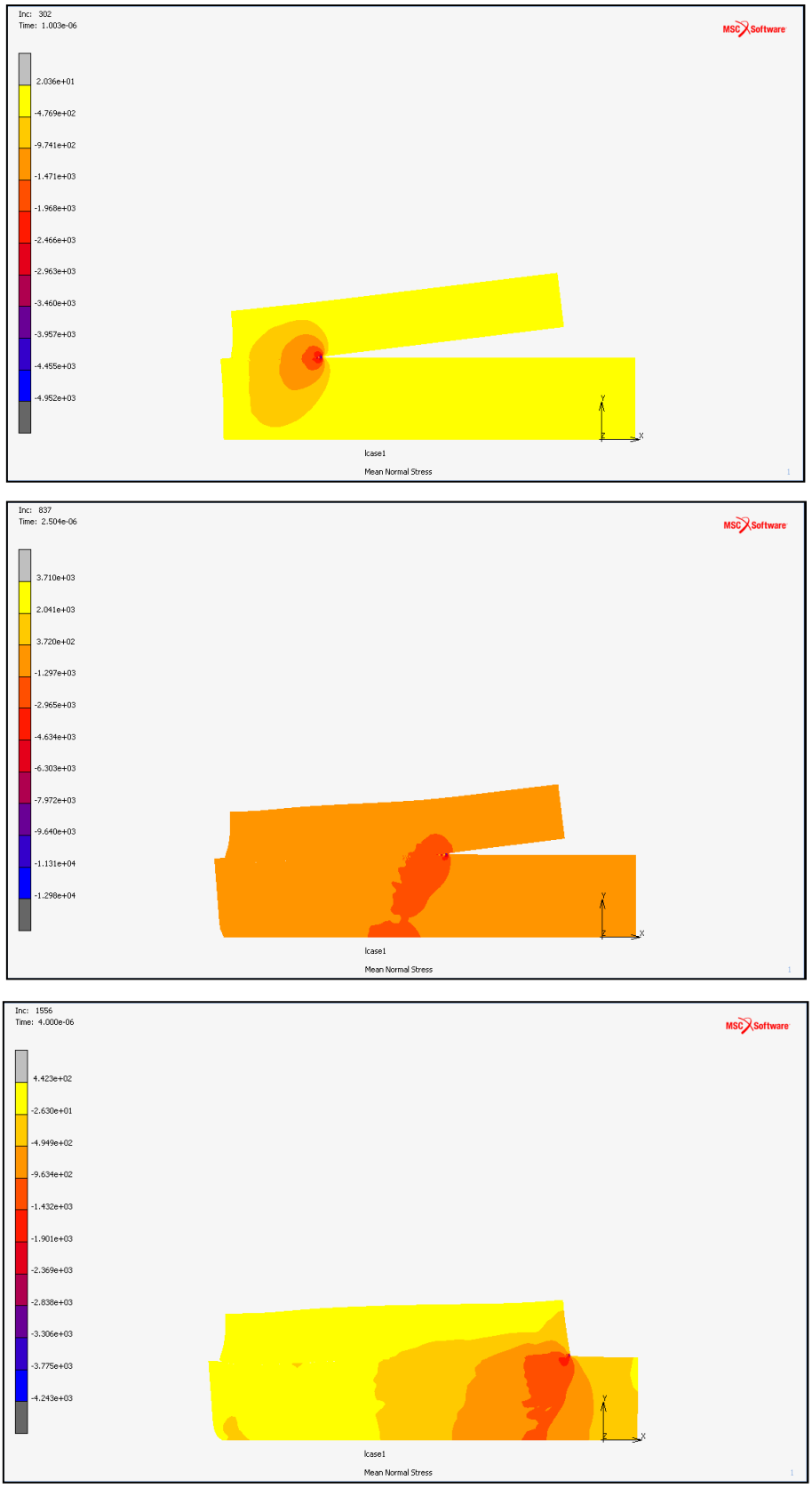

Figure 43. Pressure at 1 μs, 2.5 μs and 4 μs

2.2.6. Conclusion

To conclude, our results agree well with the results from Nassiri's article (Temperature, velocity fields, …) and the theoretical values. The small differences observed near the collision point and the interface are explained by the coarser mesh used here (additional effort should be made to achieve numerical convergence).

3. Join'EM case Study

3.1. Context and objectives

Join'EM is a 3 years frame work, that is part of Horizon 2020 initiative. H 2020 is the European research program which involves on different innovating projects. Horizon and Join'EM are in more details in the next section.

3.1.1. Horizon 2020

Horizon 2020 is the European initiative to encourage and finance research in the years to come. Under Horizon 2020 has been launched a contractual private-public partnership (PPP) named Factory of the Future (FoF). FoF aims to develop the necessary key technologies in different sectors to meet customer needs. These needs involve more sustainable, and higher customized quality products.

The goal of the Factory of the Future initiative is to combine research efforts coming from both public and private sector to provide innovation for the future. This will lead to the creation of new jobs and a leadership position for some European industries.

H2020 was approved by the European parliament and currently finances about 4300 initiatives with these 3 goals:

- Scientific excellence: Promote fundamental research and new technologies, development of research infrastructures to attract the best scientists.

- Industrial Primacy: Initiate more private investment in key technologies and emerging sectors, develop the innovative small and medium sized companies to create employment growth.
- Social Challenges: Promote innovation to reach the citizens' concerns and the European's objectives in terms of climate, environment, and energy. Develop solutions from multidisciplinary collaboration, particularly with social science.

3.1.2. Join'EM

Copper is a material that is very frequently used in today's industry because of its excellent properties, but its price has significantly increased due to the rising demand. The project Join'EM focus on copper-aluminum joining. This approach would help to decrease the copper consumption, but necessitates high quality welds which cannot be obtain using the current joining methods.

Join'EM proposes an innovative alternative to the conventional processes. Electromagnetic pulse welding is a high-speed technology for joining electrically conductive metals without mechanical contact and without heat expansion. It is possible for similar and dissimilar materials, including those which are impossible using conventional processes. EMF is a comparably new and attractive technology, which is especially promising for joining / welding, forming and cutting of tubular or sheet metal components.

Reproduced, courtesy innovaltech

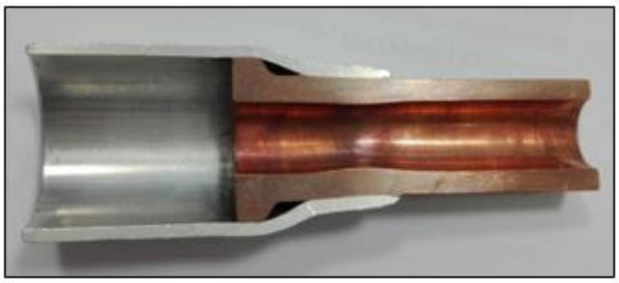

Reproduced, courtesy innovaltech

The most important aim of Join'EM is to provide the prerequisites for the industrial implementation of EMW. The advantages and benefits will be directly exploitable in series production. Join'EM will rise the TRL (Technology Readiness Level) to be closer to which the industry need. It will provide a deep knowledge and know how to develop a flexible and cost

effective magnetic joining process for metal combination where the conventional processes were found inadequate.

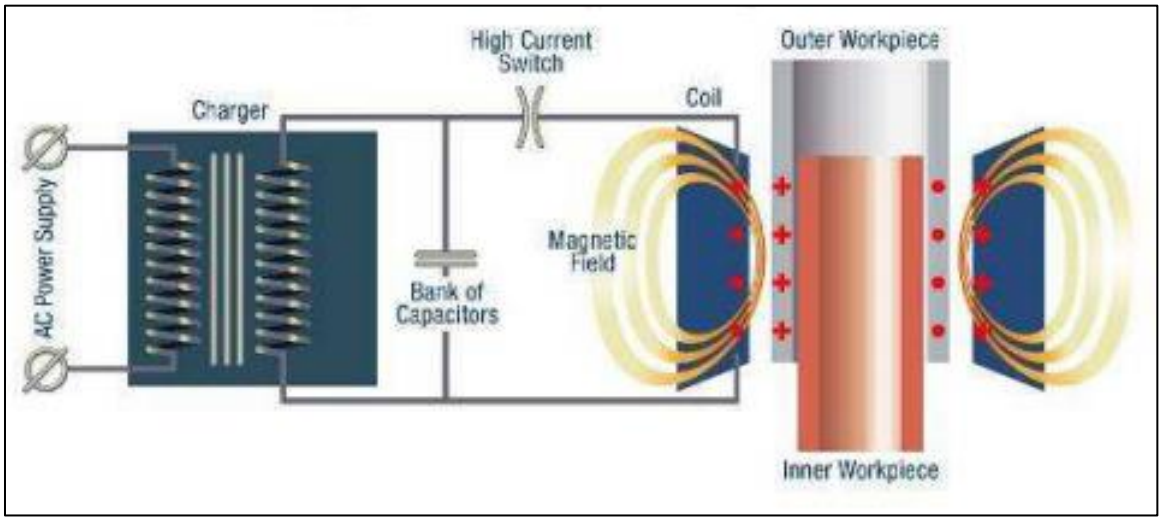

Figure 44. Process layout [5]

Join'EM involves 14 partners (figure 45).

Figure 45. Join'EM Partners

The Mechanical department of Icam Lille, is involved in work package 3:

Work package number	3	Start date or starting event									M1			
Work package title	Development of simulation strategies													
Participant number	1	2	3	4	5	6	7	8	9	10	11	12	13	14
Participant short name	FRAUNHOFER	BWI	INNOVALTECH	ARMINES	RECENDT	PHIMECA	VERTECH	EWF	WHIRLPOOL	CALYOS	CEGESA	ALKE	REfCO	ICAM
Person-months per participant	8	1	9	16		29		0.4						4.5

Figure 46. Work package 3 [18]

This work package is made up of 5 tasks:

T3.1	Macroscopic modelling of EMW: determination of acting loads, deformation and impacting conditions.
T3.2	Microscopic modelling of EMW: development of the joint formation and microstructure.
T3.3	Simulations supporting process analysis and optimization, and equipment development in WP2, 4 and 6.
T3.4	Development of a numerical lifetime prediction method for EMW equipment.
T3.5	Development of an industrial multi-scale simulation tool for modelling of EMW.

Figure 47. Purpose of the work package 3 [18]

The Mechanical department is working in T3.2 which aims to develop a microscopic simulation of the joint. This work is the translation of T3.1 and the Package 2.

Two experimental test cases are studied namely V112 and V82. These cases are described in more details in the next section.

3.2. V112 case

The first case is V112. The model details and the numerical results of this test case are given in the next section.

3.2.1. Model description

3.2.1.1. Geometry

The geometry of the V112 case (figure 48) is 2 D and composed by a base plate and a flyer plates with the dimensions of 15.5 mm by 2mm and 12mm by 2mm respectively and an impact angle $\alpha = 12.7°$ between them.

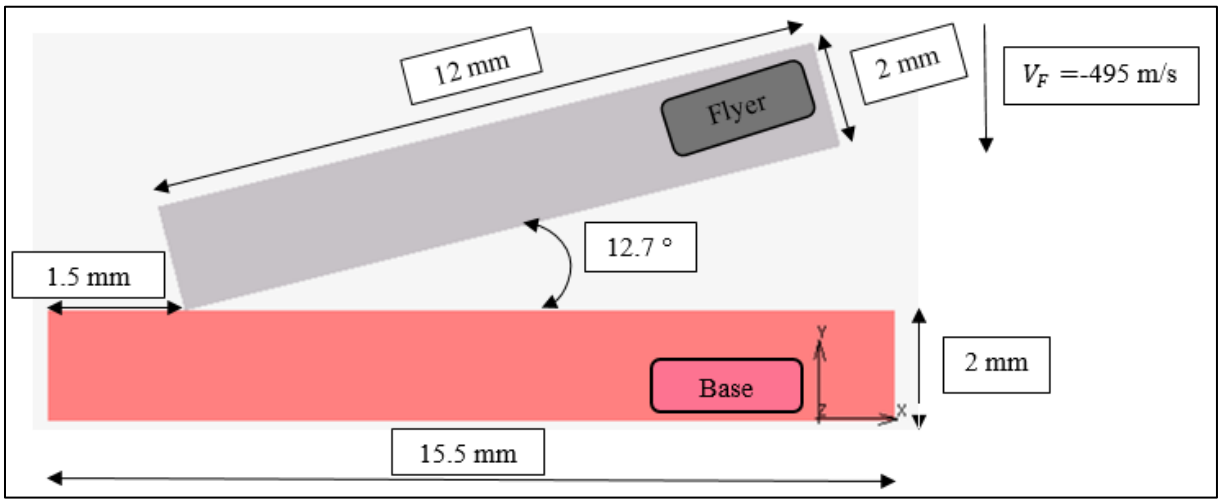

Figure 48. V112 geometry

3.2.1.2. Mesh

The mesh is made up of linear quad elements with reduce integration of 2D plane strain type. A fully coupled thermomechanical transient analyses is conducted. A global re-meshing option is used and the number of element increases from 2826 to 7025. In the end, we have the Minimum Edge Length (MEL) value is 60 μm.

3.2.1.3. Material proprieties

For the V 112 case, we used aluminum for the flyer and copper for the base. The characteristics are given in the flowing table.

Table 5. Material characteristics

Material	ρ(t/mm^3)	E(MPa)	υ	K(mW/mm/K)	C_p(mJ/t/K)	α	G(MPa)
Cu-DHP	$8.5.10^{-9}$	160000	0.33	385	383.10^{6}	$1.76.10^{-5}$	60200
EN AW-1050	$2.7.10^{-9}$	69000	0.33	229	899.10^{6}	$2.33.10^{-5}$	26000

We used the Johnson-Cook flow rule where associated parameters are given in table 6.

Table 6. Johnson-Cook parameters

Material	A(MPa)	B(MPa)	n	m	C	$\varepsilon_0(s^{-1})$	$T_{room}(K)$	$T_{melt}(K)$
Cu-DHP	200	400	0.6	1	0.012	1	296	1083
EN AW-1050	70	48	0.05	1	0.012	1	296	926

3.2.1.4. Initial and Boundary conditions

For the V112 case, the initial conditions are:

- Structural: a vertical velocity value of -495m/s imposed on the flyer.
- Thermal: a room temperature of 296 K fixed for both the flyer and the base.

The boundary conditions are the same as Nassiri case.

3.2.2. Results

The results (Plastic strain, Temperature and comparison with experience) for the V112 case are given here after.

The figure 49 shows the behavior of the plastic strain. The peak value increases from 1.6 to 3.7 at 1 μs and 7 μs respectively. This elevation induces an increase of the temperature from 480 K to 540 K between 1 μs and 7 μs (figure 50). The final temperature is 540 K which is under the melting temperature of 926 K. This result confirm that we are in the case of cold welding.

The next step is to validate our simulation with the experience done at Fraunhofer IWU. As shown in figure 51, the deformed shape close to the Fraunhofer IWU's experience: A small indentation with a shaped edge is observed at the beginning of the weld (left side) which is very similar to the experience (figure 51).

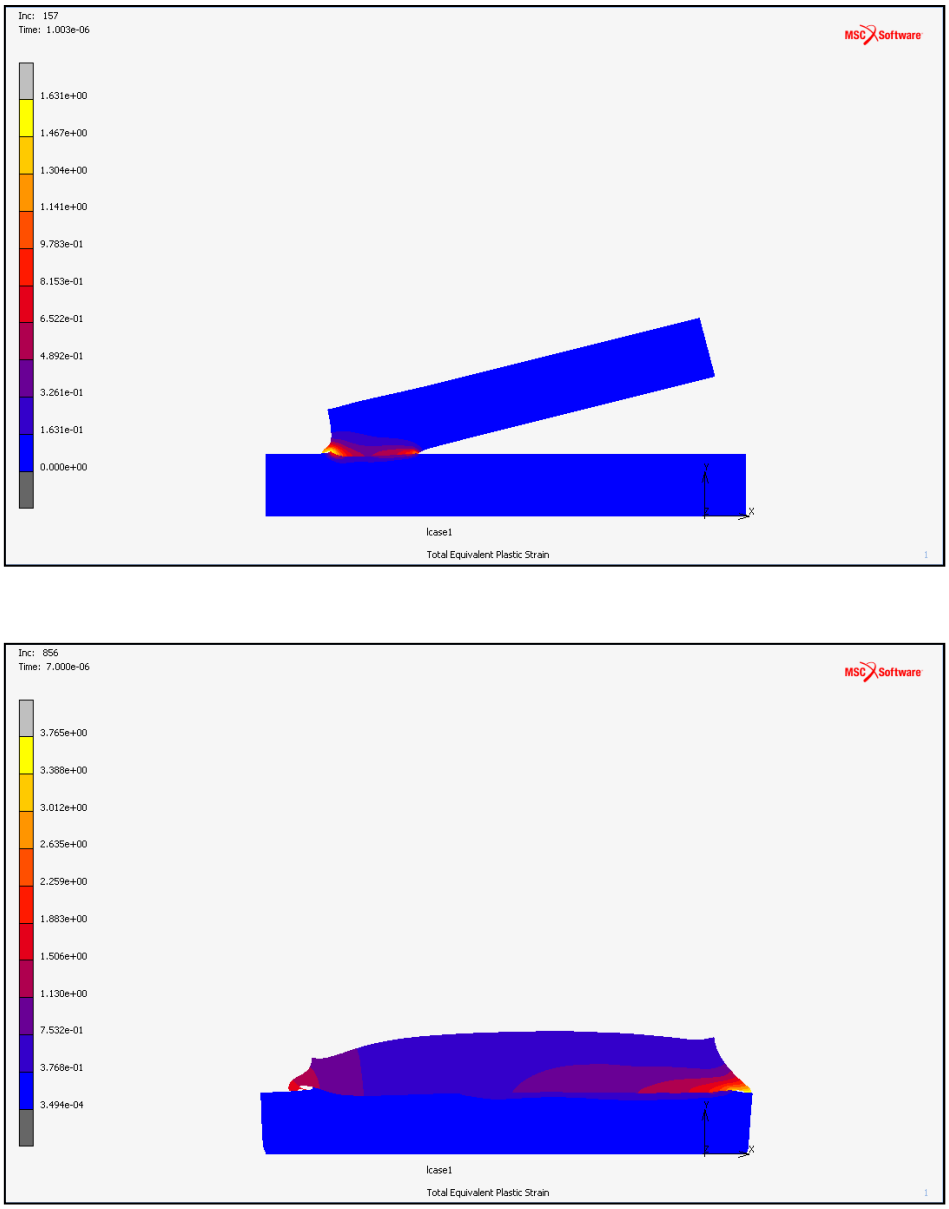

Figure 49. Effective Plastic Strain at 1 μs and 7 μs

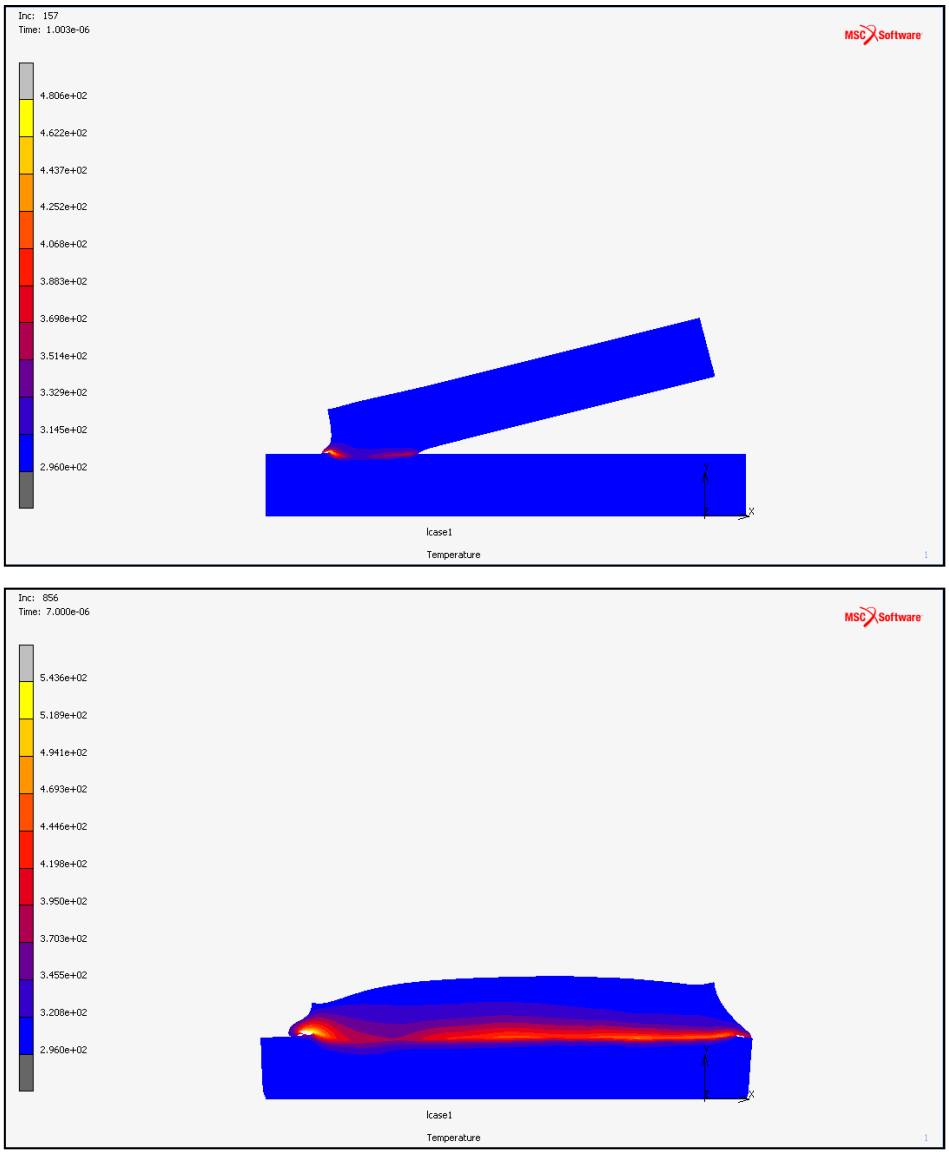

Figure 50. Temperature at 1 μs and 7 μs

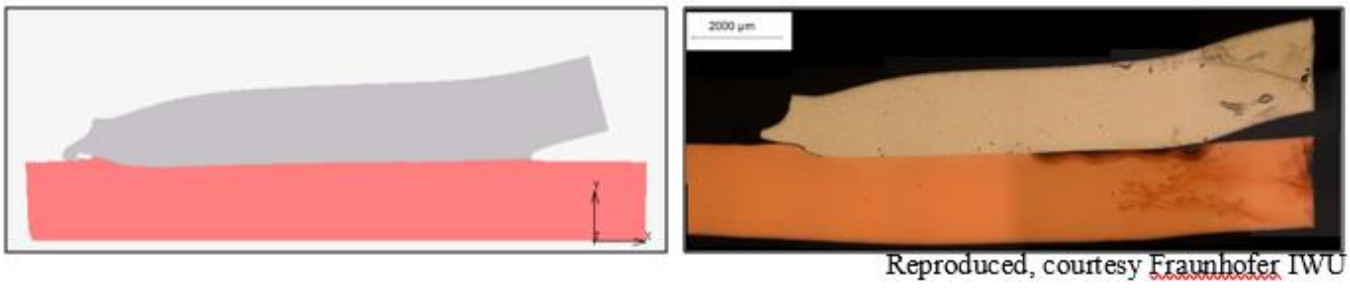

Figure 51. Comparison between a) numerical and b) experimental results

3.3. V82 Case

The second case is V82. The model details and the numerical results of this case are presented the next section.

3.3.1. Model description

3.3.1.1. Geometry

The geometry of the V82 case (figure 52) is 2 D and composed by a base plate and a flyer plates with the dimensions of 16 mm by 2mm and 15mm by 2mm respectively and an impact angle $\alpha = 14.18°$ between them.

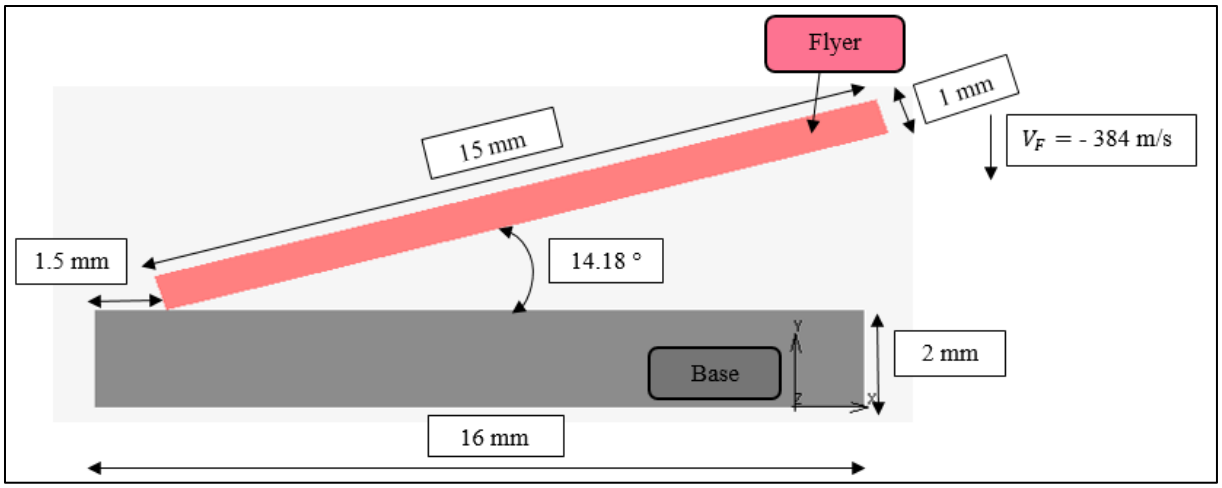

Figure 52. V82 Geometry

3.3.1.2. Mesh

The mesh is made up of linear quad elements with reduce integration of 2D plane strain type. A fully coupled thermomechanical transient analyses is conducted. A global re-meshing option is used and the number of element increases from 2227 to 4620. In the end, we have the Minimum Edge Length (MEL) value is 45 μm.

3.3.1.3. Material proprieties

For V 82 case, we used aluminum for the base and copper for the flyer. The material proprieties are the same as in V112 case.

3.3.1.4. Initial and Boundary conditions

For V82 case, the initial conditions are:

- Structural: a vertical velocity value of -384 m/s imposed on the flyer.
- Thermal: a room temperature of 296 K fixed for both the flyer and the base.

The boundary conditions are the same as Nassiri case.

3.3.2. Results

The results (Plastic strain, Temperature and comparison with experience) for the V82 case are given here after.

The figure 53 shows the behavior of the plastic strain. The peak value increases from 1.3 to 3.3 at 1 μs and 7 μs respectively. This elevation induces an increase of the temperature from 360 K to 425 K between 1 μs and 10 μs (figure 54). The final temperature is 425 K which is under the melting temperature of 926 K. This result confirm that we are in the case of cold welding.

The next step is to validate our simulation with the experience done at Fraunhofer IWU. As shown in figure 55, the deformed shape close to the Fraunhofer IWU's experience: A small separation with a shaped edge is observed at the beginning of the weld (left side) which is very similar to the experience (figure 55).

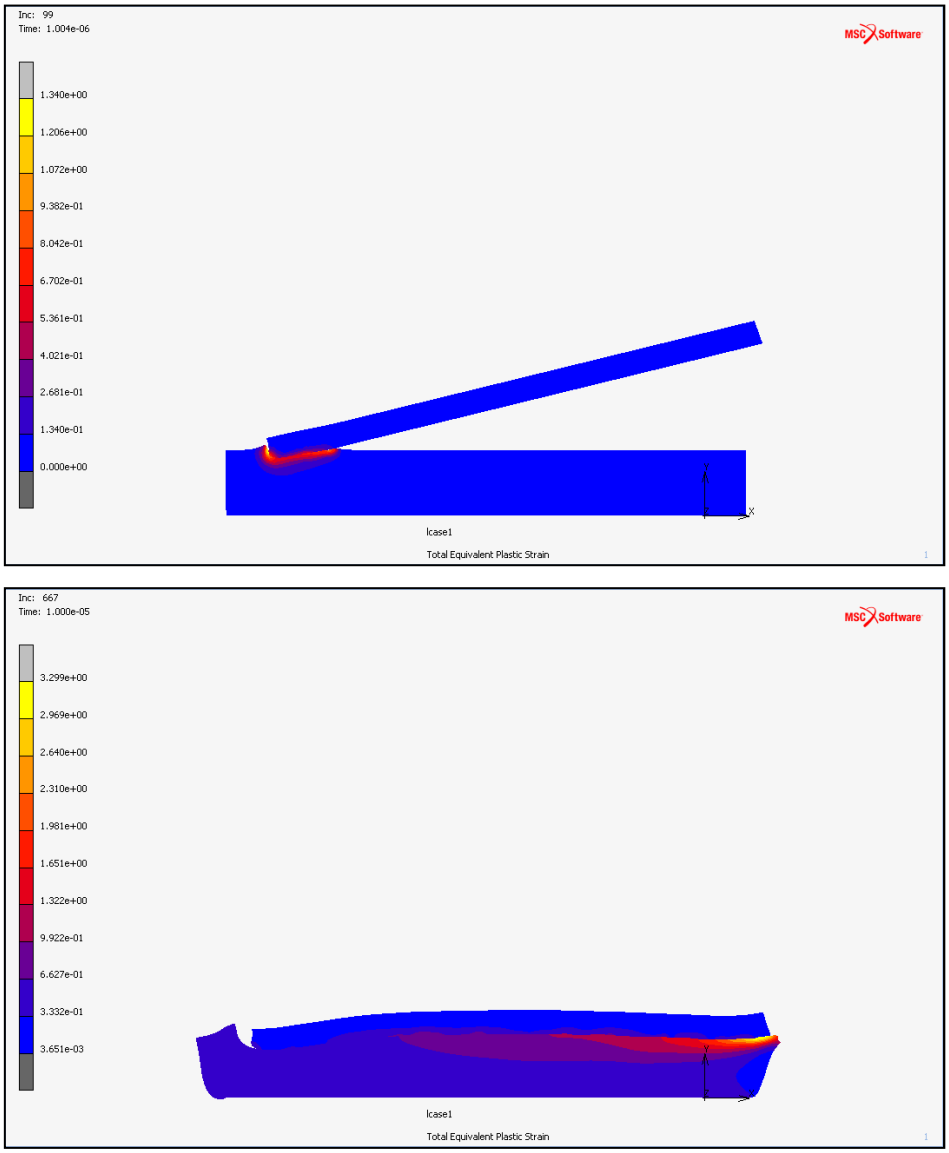

Figure 53. Effective Plastic Strain at 1 μs and 10 μs

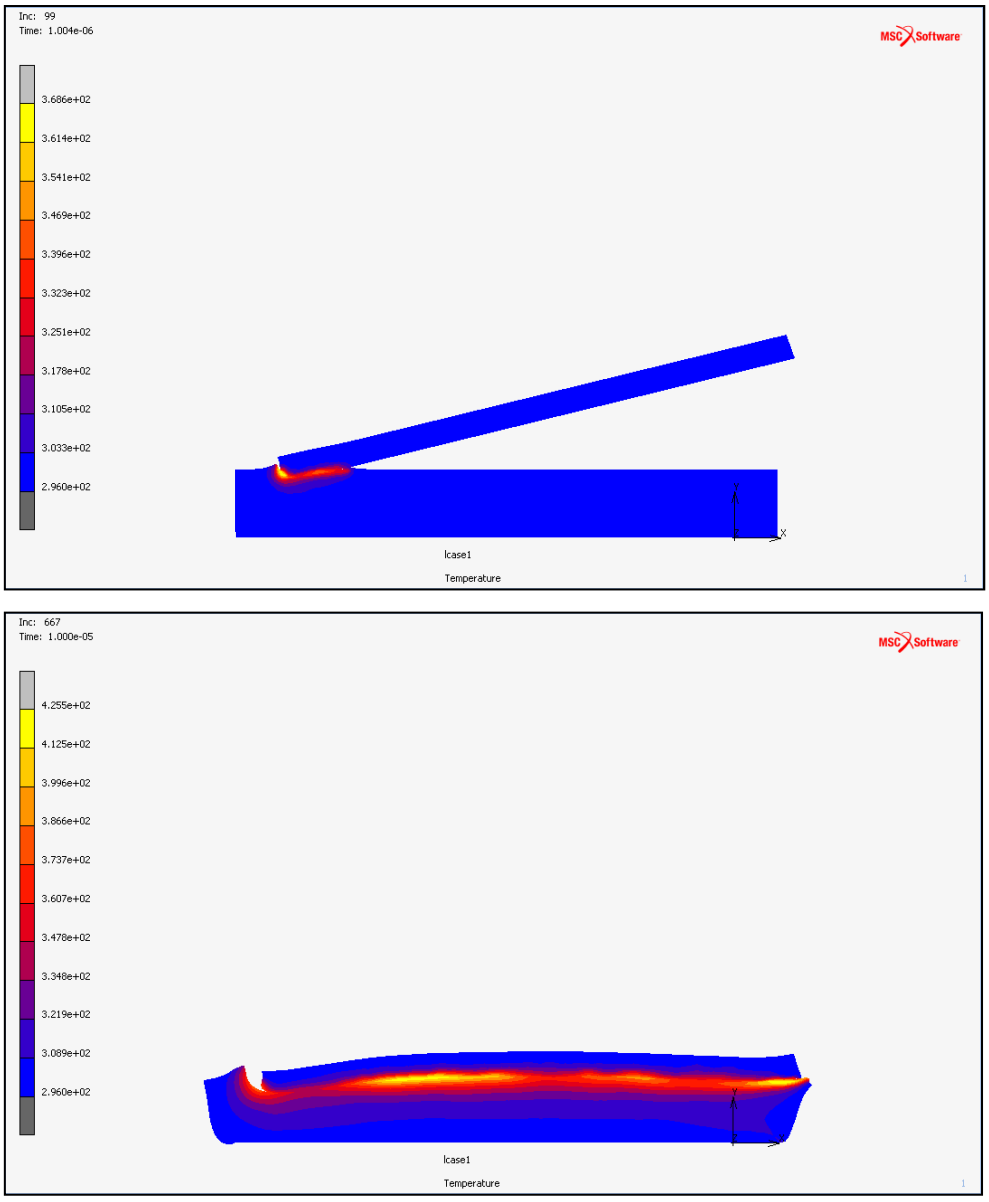

Figure 54. Temperature at 1 μs and 10 μs

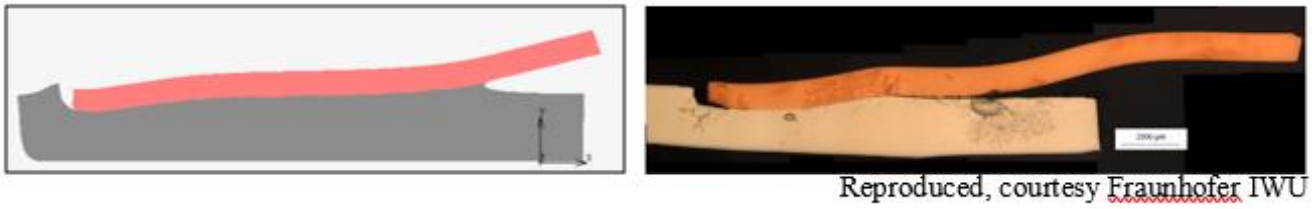

Figure 55. Comparison between a) Numerical and b) experimental results

3.3.3. Jet

The figure 56 show the simulation result near the Collison point for Al/Al, Al/Cu and Cu/Al configuration. The properties of the materials were given in the previous sections. The composition of the metal jet can be classified according to the densities of the two metal plates. In the case of a large density difference such as Al/Cu and Cu/Al lap joints, the metal jet is mainly composed of the lower density material. On the other hand, when the density difference is zero, such as for Al/Al lap joints, the metal jet is composed of both plates.

The figure 26 shows also that our results are comparable to the literature [6].

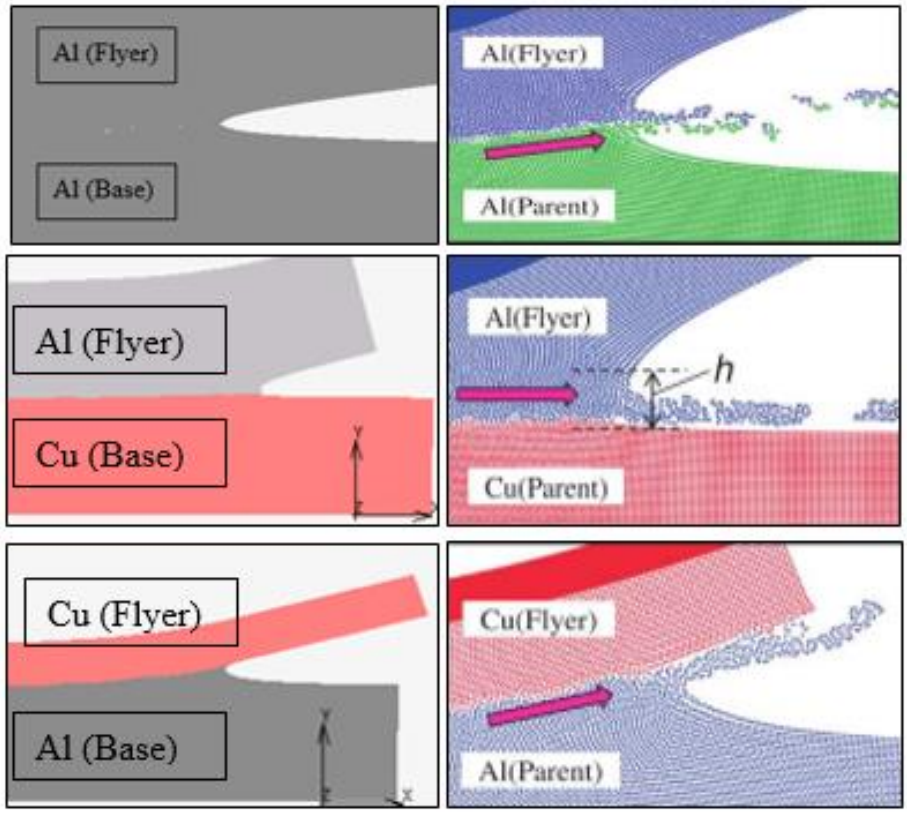

Figure 56. Comparison of the jet between a) our result and b) the literature [19]

Of course, due to the large MEL and some limitations in remeshing technologies, the jet in our case could not be captured well compared to SPH simulations [19].

4. Conclusion

In this chapter, we studied Nassiri and Join'EM cases. In both cases, our results are encouraging when comparing with the literature and the experience. In both cases, we have to reduce the Minimum Edge Length (MEL) in order to have results closer to theses coming from the literature and the experience.

In the next chapter, second part of this project is presented namely fusion welding.

Chapter 4:

Fusion welding

1. Introduction

Multi-pass welding (Metal Deposition) process is similar to Additive Manufacturing (AM) which is an appropriate name to describe the technologies that build 3D objects by adding layer-upon-layer of material. Many types exist: Rapid Prototyping (RP), Direct Digital Manufacturing (DDM), layered manufacturing, etc. In this chapter, we study multi-pass (Metal Deposition MD) welding process (figure 57). The aim of this process is build up features or even complete components with wanted geometry.

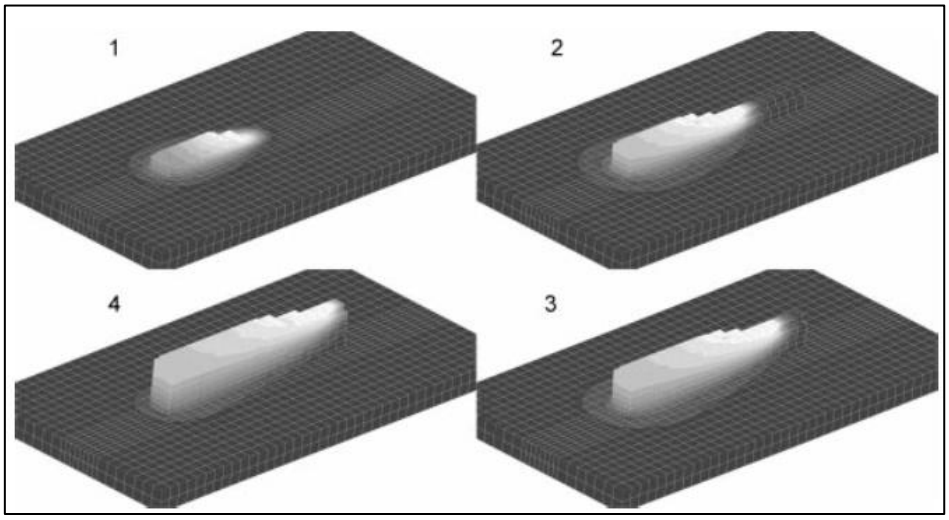

Figure 57. Metal deposition process principle (white denotes the highest, melting temperature, and black is room temperature) [20]

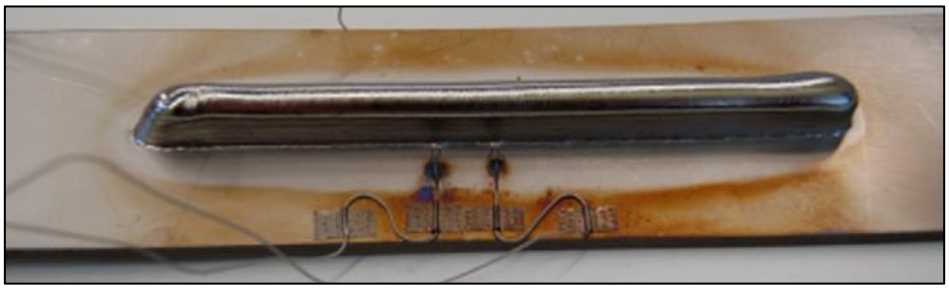

Figure 58. Metal deposition process [21]

The goal of this study is to study the feasibility of modeling a metal deposition process. To do, we take the article of lundbäck & al [21] as a reference.

For this study, like impact welding, we use MSC software with Marc as solver and Mentat as pre- and post-processor to carry out a transient thermo-mechanical simulation.

The unit system used is mm/tonne/s/°C.

2. Model description

The model description and the results are depicted more in details bellow.

2.1. Geometry/ Mesh

The geometry/mesh is built in 3 D (Figure 59). The size of the base plate is 200mm×50mm with a thickness of 3.2mm. The material isn't mentioned so we used the material in use other MSC test case of fusion welding.

So, the material chosen for the base is 100 Cr 6 where the characteristics come from the material library of Marc.

The deposited material is made up of 9 layers of 1 mm thickness (figure 59). The dimensions of the deposited material are 140mm×8mm×9mm and the material is 41Cr 4 where the characteristics come also from Marc's Library.

A heat transfer transient simulation has been carried out first.

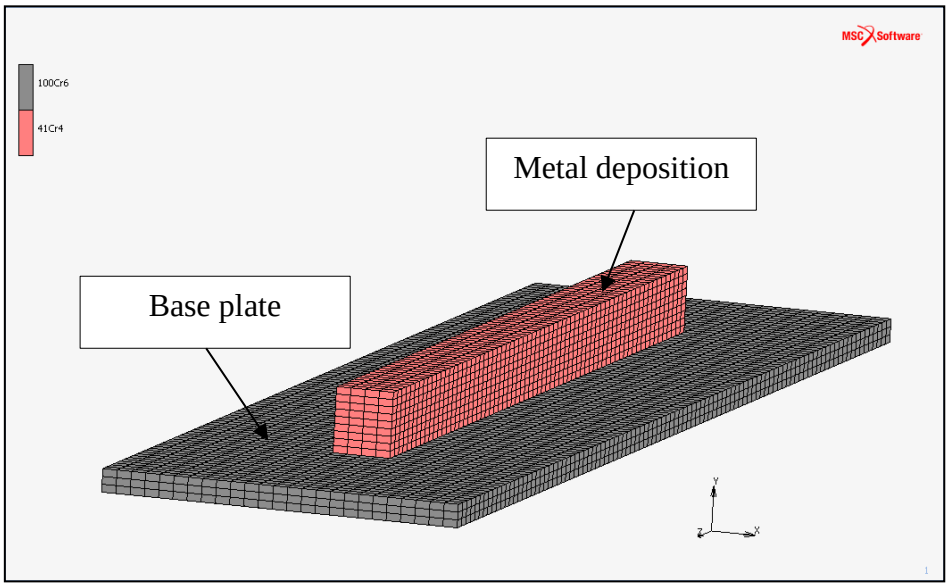

Figure 59. FE-model, single wall with 9 layers

The parameters of the physical process are shown in table 7. The nominal power input is given by the current I, times the voltage, U. The weld speed v_{weld}, the feed rate of the wire v_{wire} and the diameter of the wire $\emptyset_{wire}$.

For the heat input model, the double ellipsoid shaped weld heat source of Goldak is used [22]:

$$q_f(x,y,z) = \frac{6\sqrt{3}f_f Q}{abc_f\pi\sqrt{\pi}} \exp\left(\frac{-3x^2}{a^2}\right) \exp\left(\frac{-3y^2}{b^2}\right) \exp\left(\frac{-3z^2}{c^2}\right)$$

$$q_r(x,y,z) = \frac{6\sqrt{3}f_r Q}{abc_r\pi\sqrt{\pi}} \exp\left(\frac{-3x^2}{a^2}\right) \exp\left(\frac{-3y^2}{b^2}\right) \exp\left(\frac{-3z^2}{c^2}\right)$$

where q_f and q_r are the weld flux rates per unit volume in the front and rear weld pools respectively; Q= η *U*I is the applied power; a is the weld width along the tangent direction x; b is the weld penetration depth along the arc direction y; c_f and c_r are the forward and rear weld pool lengths in the weld path direction z; f_f and f_r are dimensionless factors given by

$$f_f = \frac{2}{(1 + c_r/c_f)}$$

$$f_r = \frac{2}{(1 + c_f/c_r)}$$

The double ellipsoid source is shown below (figure ??).

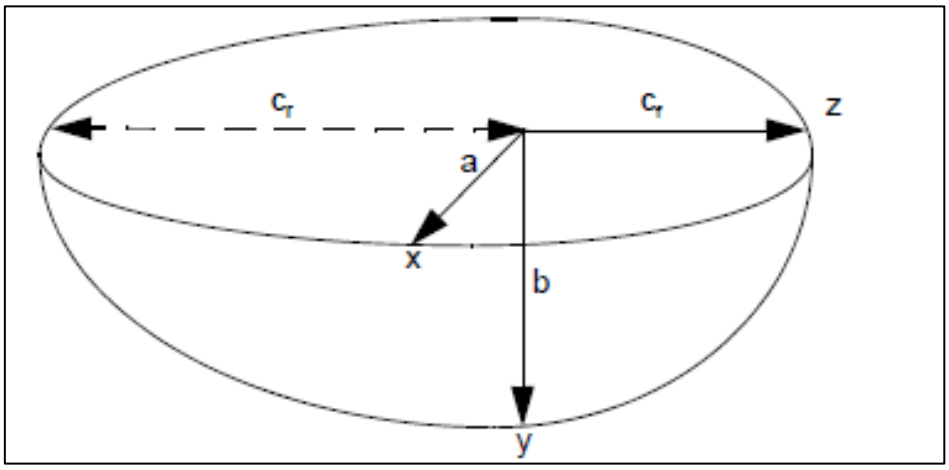

Figure 60. Double ellipsoidal heat source [22]

The heat source parameters a, b, c_f, c_r, the convective heat loss h, the emissivity e and the efficiency of the heat input η are given in table 8.

Table 7. Process parameters [21]

I (A)	U (V)	v_{weld} (m/s)	v_{wire} (m/s)	$\emptyset_{wire}$ (m)
87	10.3	0.002	0.0125	0.00114

Table 8. Estimated parameters [21]

h ($Wm^{-2}K^{-1}$)	e	η	a (m)	b (m)	c_f (m)	c_r(m)
18	0.88	0.58	0.004	0.0012	0.004	0.006

2.2 Initial conditions

The initial thermal condition is in a room temperature of 20°C fixed for all the degree of freedom (figure 61).

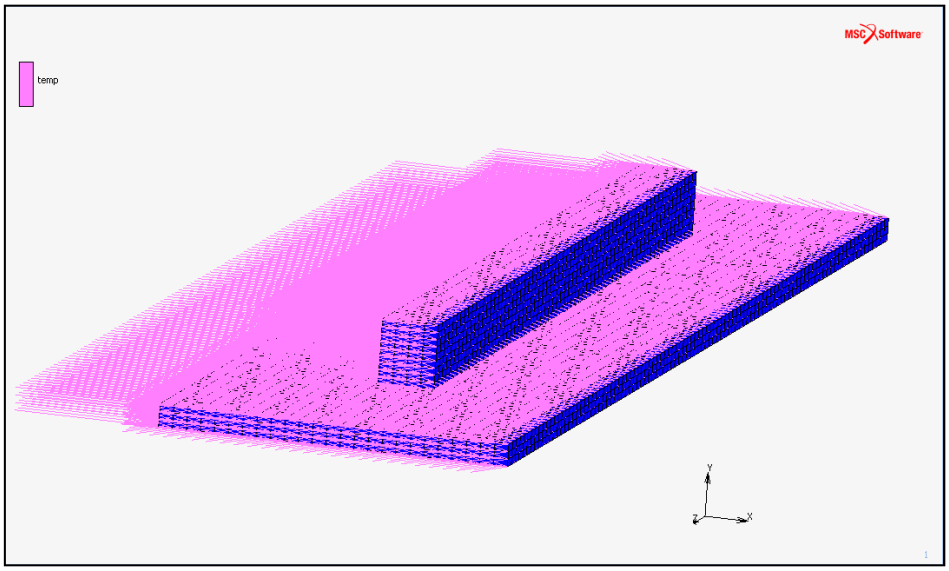

Figure 61. Initial condition

2.3 Boundary conditions

In this study, we have three types of boundary conditions: fixed temperature, face film and weld flux. These boundary conditions are given in more details in the following section.

2.3.1. Fixed temperature

The first boundary condition is to fix a temperature of 20 °C at the bottom of the base plate as illustrated in figure 62.

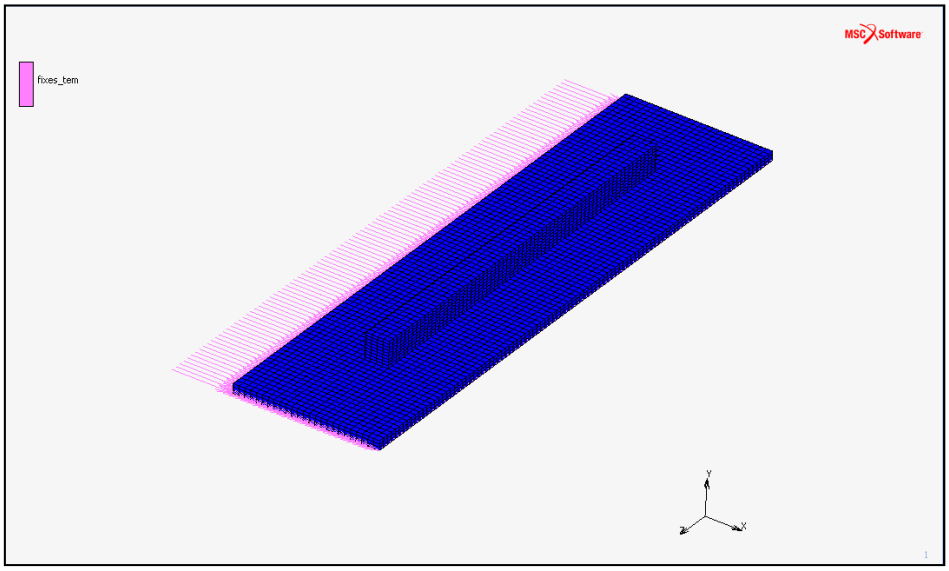

Figure 62. Fixed temperature

2.3.2. Face film

This condition is necessary to model the convective and radiation heat exchanges. We applied this condition for each layer. The face film for the final layer is illustrated in figure 63.

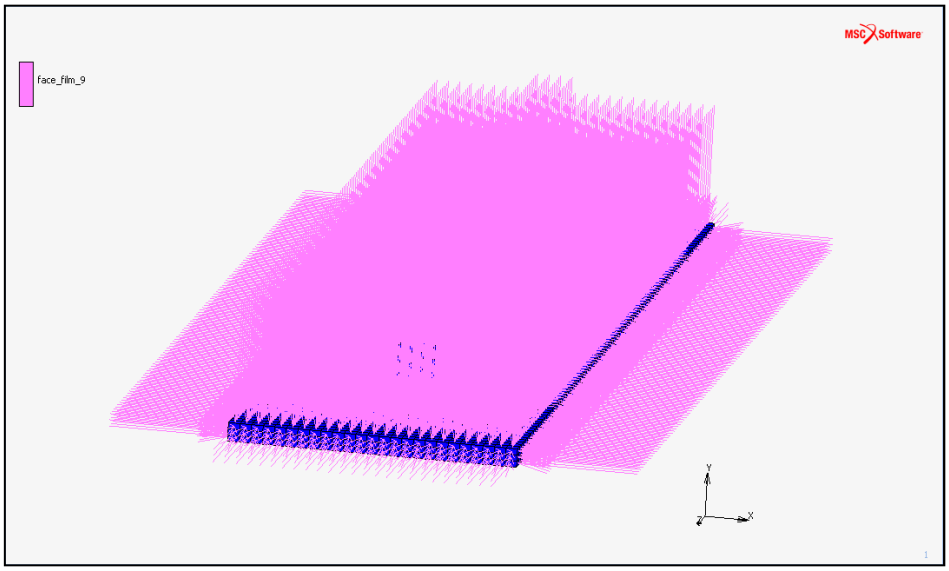

Figure 63. Face film

2.3.3. Weld Flux

Welding is a thermal process with specific boundary conditions. These boundary conditions are specified through the weld Flux model definition option in conjunction with the Weld Path and Weld Fill options.

- Weld Flux

It can be a double ellipsoidal shaped volume heat source, or a cylindrical shaped. In our case, we used a double ellipsoidal source (figure 60).

The total heat input applied through the weld flux should be equal to the electrical power:

$Q = \eta * U * I$.

- Weld Path

The path followed by the welding heat source and the orientation of the weld arc are specified by the Weld Path model definition option. This information is used to determine a local coordinate system for the moving source, as shown in figure 64. The weld path vector is taken as the local z axis. The arc orientation vector is taken as the local y axis. The tangent vector that is perpendicular to both y and z axes defines the local x axis.

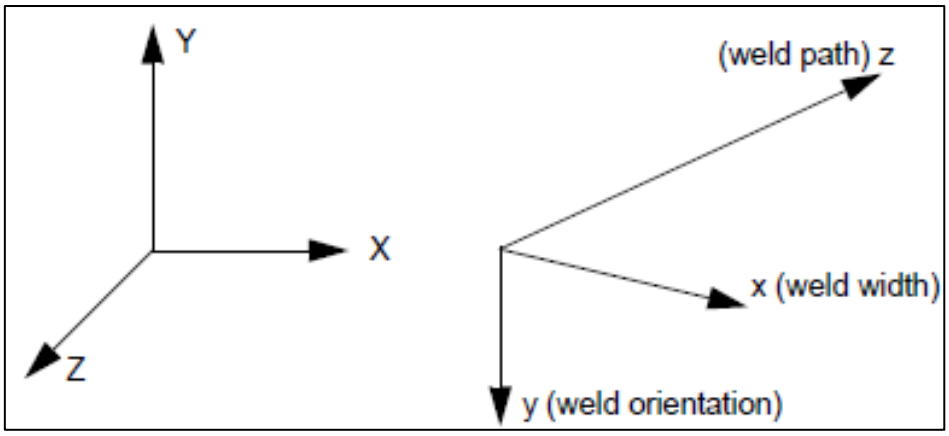

Figure 64. Local coordinate system for moving source obtained by translation and rotation of global coordinate system [22]

In our study, we applied a weld path for each layer and all the weld path are illustrated in figure 65.

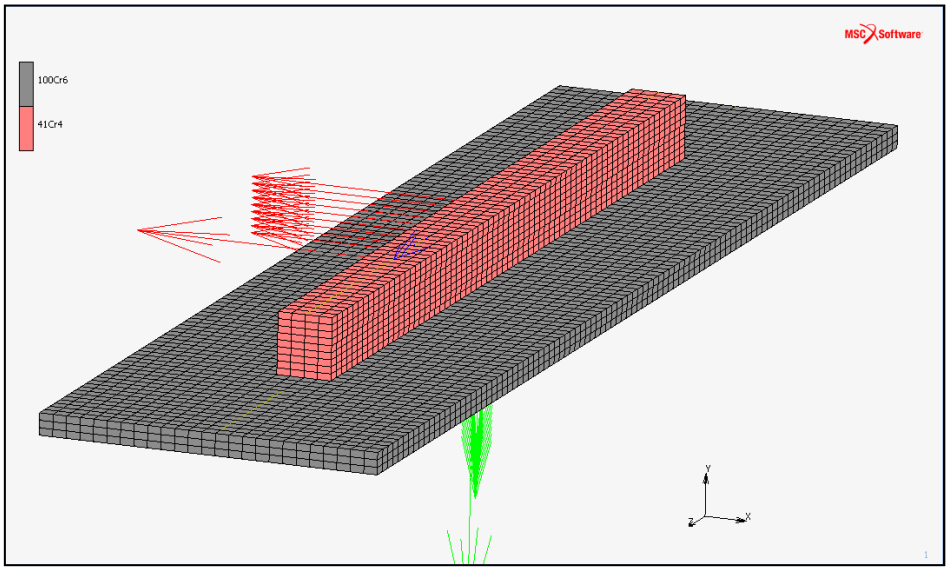

Figure 65. Weld Path

- Weld Fill

The dynamic creation of filler elements and the generation of associated boundary conditions is defined by the Weld Fill model definition option.

Two methods are supported for the creation of filler elements:

- ✓ Quiet element: the elements are present in the analysis but are assigned properties so they don't affect the analysis.
- ✓ Inactive element: the elements are included in the analysis until the corresponding material has been added.

Like all methods, Quiet and Inactive methods present advantages and disadvantages which are illustrated in table 9.

Table 9. Advantages and Disadvantages of Quiet and Inactive Methods

	Advantages	Disadvantages
Quiet	-It is easy to implement and can be applied to commercial finite element codes via user subroutines. -Since the number of element does not change, the number of equations is constant through the analysis and no additional equation renumbering and solver initialization is needed.	-Implementation of the quiet element method in modeling additive manufacturing, where most of the analysis domain is composed of quiet element, may result into long computer runs.
Inactive	-There are no errors introduced by scaling factors as is the case of the quiet element. -Only the active nodal degrees of freedom are considered at a time of the resolution.	-The method cannot be easily incorporated into general purpose commercial codes using user subroutines. -The equation numbering and solver initialization have to be repeated every time elements are activated. This may negate the computational advantage of solving for a reduced active number of degree of freedom.

According to Michaleris [23], there is a new hybrid inactive/quiet element method. In this method, initially the element corresponding to metal deposition are inactive, then they switched to quiet on a layer-by-layer basis.

In our simulation, we used an inactive element method and the weld Flux of the layer number 9 is illustrated in figure 66.

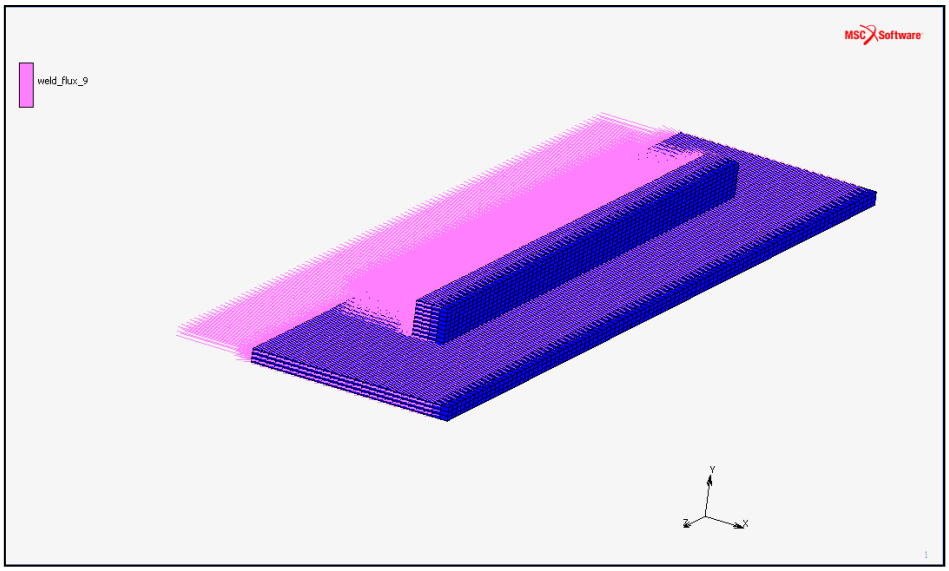

Figure 66. Weld Flux

In our simulation, we associated a local remeshing with the moving heat source. The Minimum edge length decreases from 2 μm to 1 μm in order to capture better the temperature gradients.

3. Results

The figure 67 shows the multi-pass welding process: the addition of the metal deposition from layer to layer (layer 1, 5 and 9). This result is similar to Lundbäck & al ‘s [21] model shown in figure 57.

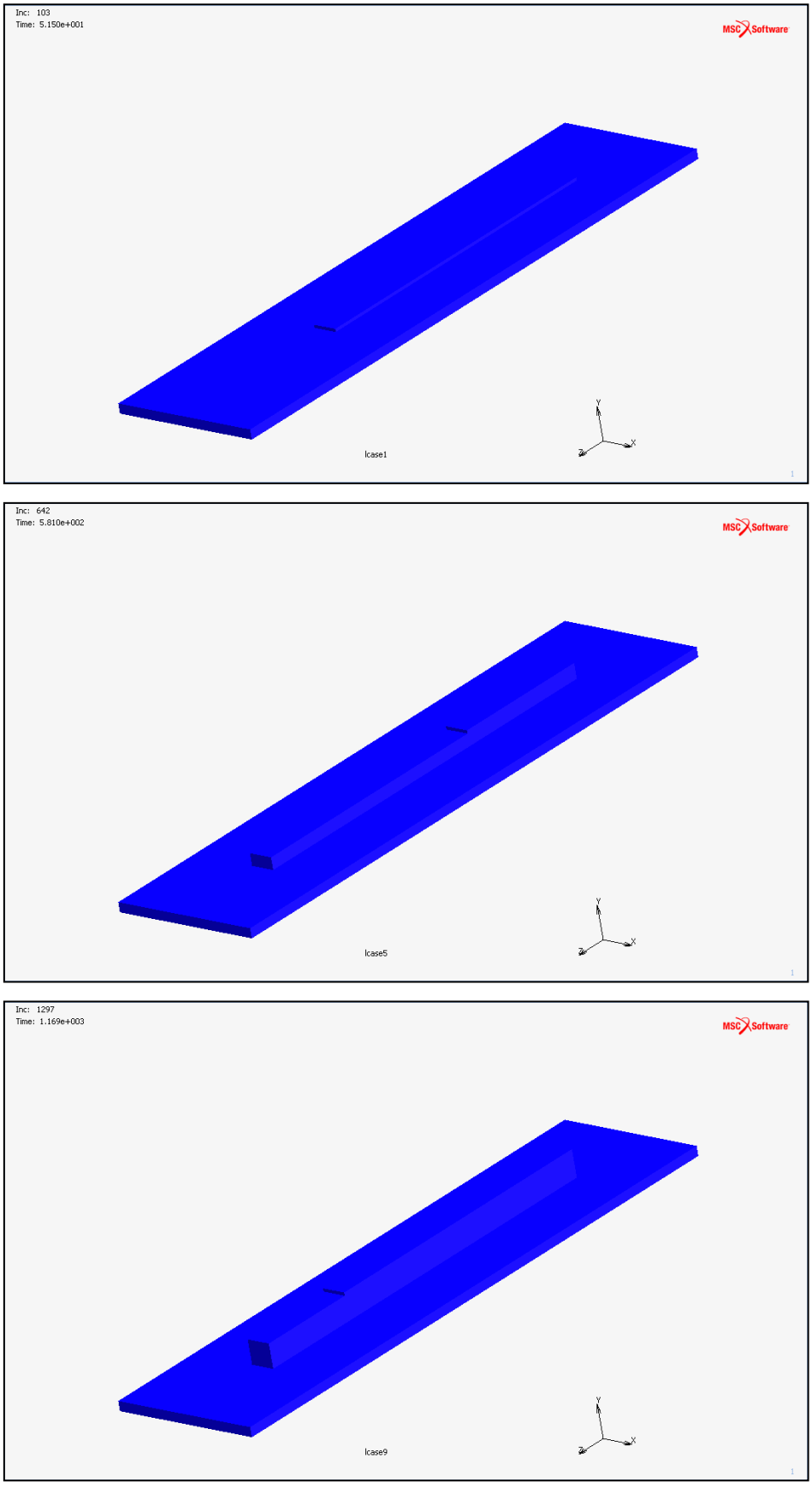

Figure 67. Multi-pass welding process in layers 1, 5 and 9

The figure 68 shows the temperature distribution for the arc welding process (layer 5 and layer 9). As shown in the figure below, the max temperature during our simulation is about 1500 °C.

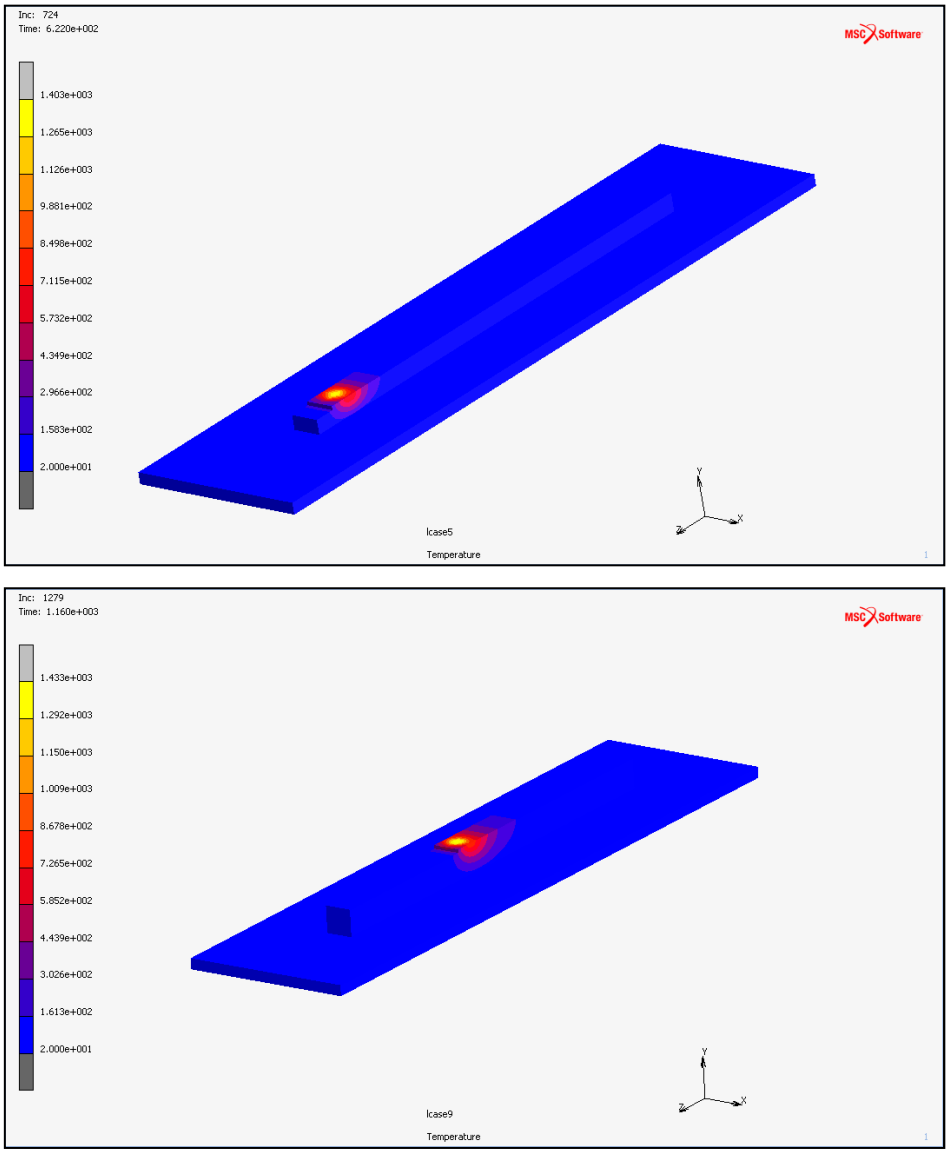

Figure 68. Temperature in layers 5 and 9

In figure 70, the calculated temperature history during a metal deposition process (9 pass) for a node in contact between the base plate and the first layer (figure 69), is given.

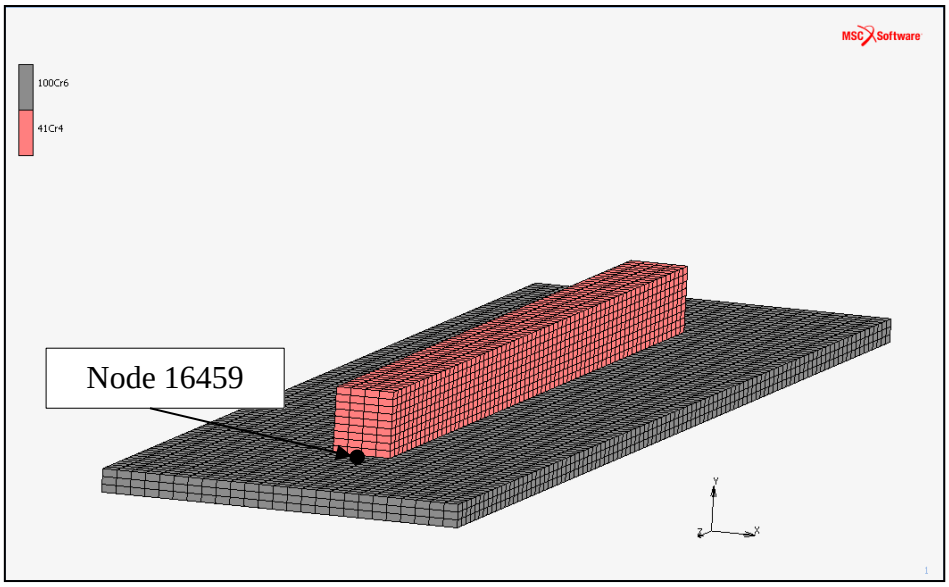

Figure 69. Position of the node 16459

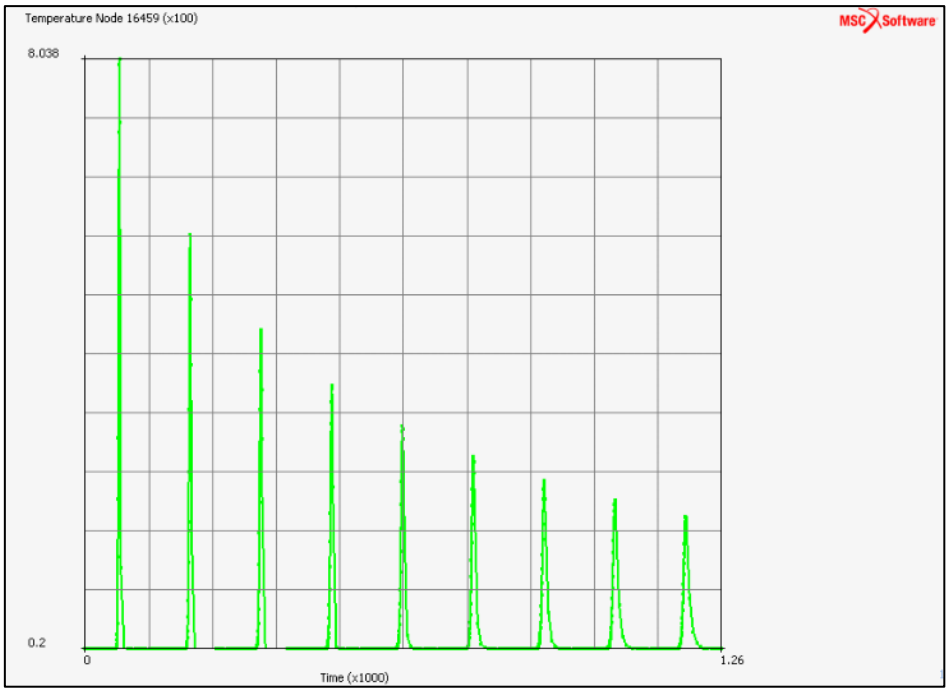

Figure 70. Computed temperature history

The temperature decreases from 800 °C to 20 °C for the first layer. Although, in figure 67 we have 1500°C. This difference is due to heat transfer by conduction, convection and radiation. Also, the value of temperature decreases from layer to layer which is logical: the heat source departs from the node selected for each layer. This behavior is closer to the Lundbäck& al's simulation [21].

Figure 70 shows also a constant temperature of 20°C between each layer. This temperature is due to the time made from layer to layer. This last is to make the weld cooling.

4. Thermo-mechanical simulation

The goal of this study is to simulate a transient thermo-mechanical simulation. For that we added a boundary conditions which are:

- Fixed displacement (figure 71)
- Gravity load (figure 72)

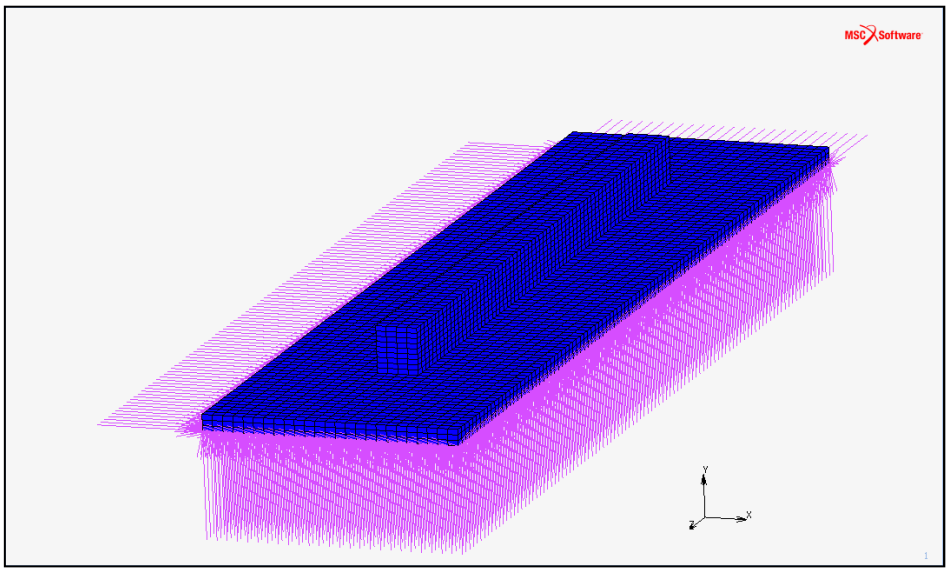

Figure 71. Fixed displacement

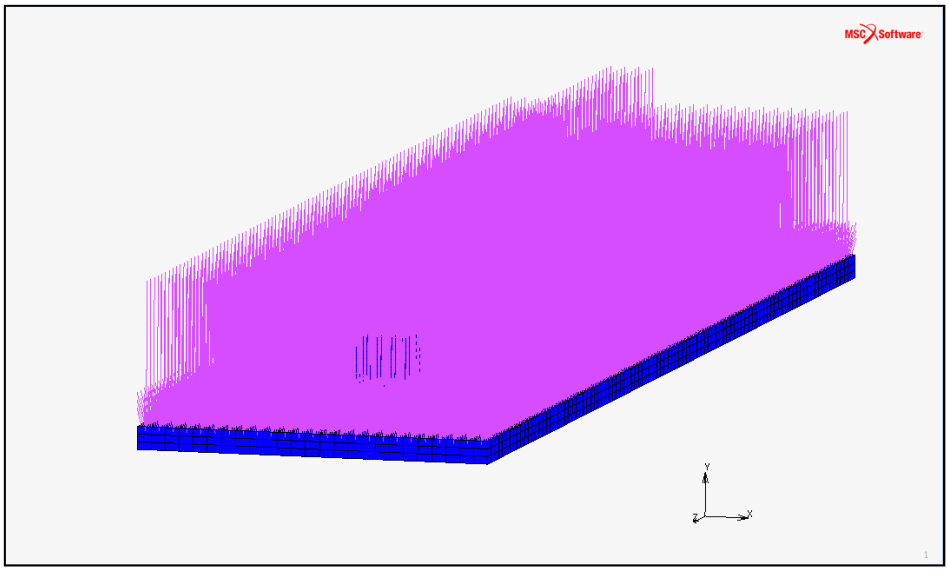

Figure 72. Gravity load

For the thermo-mechanical simulation, unfortunately we don't have enough time to achieve this goal. But in parallel, we did an experience in Icam's workshop to illustrate the arc welding. The result is shown in figure 73.

Figure 73. Process illustration

This process illustration is just to show the process and if we want to validate our simulation, we should also add a thermocouple or pyrometer to measure the value of the temperature. Also, we should add a thermal camera to visualize the temperature field.

5. Conclusion

In this chapter, we studied the fusion welding in order to study the feasibility of the process. The results of the thermal simulation are encouraging with the literature. But For thermo-mechanical simulation, until now, we don't have good results. For that, we aim to have in future good results and to validate them with the experience.

General conclusion

This paper is the conclusion of 5 month of work in the mechanical department of Icam school in Lille. The goal of this project is to study thermo-mechanical behavior of two industrial process: Impact and fusion welding.

First, a literature review has been realized to understand well the welding process in general and how to simulate impact and fusion welding.

After that, we simulate the impact welding with Marc Mentat. Two cases are studied: Nassiri case where our results are close to his results. The goal of this study is to calibrate our methodology. The second case is Join'EM which is a H2020 European project. For the Join'EM case, two benchmarks are studied: V112 and V82. For both cases, our results are similar to the experience done by Fraunhofer IWU.

The final part of this project is dedicated to fusion welding. In this study, our results for heat transfer analysis are encouraging but for thermo-mechanical simulation, we don't have yet good results.

In this internship, we participated to the MSC contest, June 2017, which is an annual contest where the customers participate with their demonstration of using MSC's software simulation technology. Also, we participated to Join'EM project newsletter #2 and finally with an article to CFM (French Congress of Mechanics), Lille 2017.

Thanks to the in-depth knowledge acquired during our training and the continued encouragement of our supervisors, we have succeeded in accomplishing our work. This internship allowed us to solve advance numerical problems and to conduct for the first-time research in the field of computational welding mechanics autonomously.

Perspectives

After the thermo-mechanical simulation in 2D sheet metal of impact welding. We aim in first time to make the mesh more refined to achieve results closer to the reality. We aim, then, to study a 2D axisymmetric simulation of Join'EM case, a 3D simulation and multiphasic simulation (Magneto-dynamic, Structural, Thermal).

For fusion welding, we aim in first time to solve the problem of the thermo-mechanical simulation and then to validate our simulation with an experience where we add a thermocouple or pyrometer to measure the temperature and a thermal camera to visualize the temperature field.

Bibliography

[1@] https://www.icam.fr

[2] MECHANICAL ENGENIEERING, Welding Joints and Symbols

[3] A. Nassiri, G. Chini, A. Vivek, G. Daehn, and B. Kinsey, "Arbitrary Lagrangian–Eulerian finite element simulation and experimental investigation of wavy interfacial morphology during high velocity impact welding," *Mater. Des.*, vol. 88, pp. 345–358, Dec. 2015.

[4] S. R. Reid, "A discussion of the mechanism of interface wave generation in explosive welding," *Int. J. Mech. Sci.*, vol. 16, no. 6, pp. 399–413, 1974.

[5] V. Shribman, "Magnetic pulse welding of automotive HVAC parts," Rapp. Tech. Pulsar Ltd, 2007.

[6] H. Gallizzi,"Etude et application des champs magnétiques intensrs au soudage d'éléments turbulaires en acier oxydables", Rapport CEA, .1986

[7] W. Antunes, Milton. Lima,"Etude et application des champs magnétiques intensrs au soudage d'éléments turbulaires en acier oxydables", Soldag. insp. vol.21 no.3 São Paulo July/Sept. 2016.

[8] Dr. Dmitri Kopeliovich, Principles arc welding.

[9@] http://www.weldingengineer.com/1mig.htm

[10@] http://nptel.ac.in/courses/112107144/34

[11@] http://www.steelconstruction.info/Welding

[12@] http://www.welderreferer.com

[13@] http://www.the-warren.org/GCSERevision/engineering/soldering.html

[14] L.-E. Lindgren, "Numerical modelling of welding," Comput. Methods Appl. Mech. Eng., vol. 195, no. 48–49, pp. 6710–6736, 2006.

[15] Böllinghaus, T., Byrne, G., Ilich, B., Chlebus, E., Cross, C. E., Denkena, B., … Woeste, K. (2009). Manufacturing Engineering. Handbook of Mechanical Engineering, 523–785.

[16] H. Serizawa and I. Shibahara, "Numerical Study of Joining Process in Magnetic Pressure Seam Welding," Trans. JWRI, vol. 38, no. 1, pp. 63–68, 2009.

[17] Guglielmetti, A. (2012). Thèse de Doctorat : Etude numérique du soudage par impulsion magnétique.

[18] P. S. Forms, “Horizon 2020 Call: H2020-FoF-2014 Topic: FoF-04-2014 Type of action: IA Proposal number: SEP-210152839 Proposal acronym : HuManPlace,” 2014.

[19] S. Kakizaki, M. Watanabe, and S. Kumai, “Simulation and experimental analysis of metal jet emission and weld interface morphology in impact welding,” J. Japan Inst. Light Met., vol. 61, no. 7, pp. 328–333, 2011.

[20] Lindgren, L.-E. (2007). computational welding mechanics thermomechhanical and microstructurall simulations.

[21] Lundbäck, A., & Lindgren, L. E. (2011). Modelling of metal deposition. Finite Elements in Analysis and Design, 47(10), 1169–1177.

[22] Volume A: Theory and User Information, Marc

[23] Michaleris, P. (2014). Modeling metal deposition in heat transfer analyses of additive manufacturing processes. Finite Elements in Analys